Relationships linking satellite-retrieved ocean color data with atmospheric components in the Arctic

Marjan Marbouti[1,2], Sehyun Jang[3], Silvia Becagli[4,6], Gabriel Navarro[5], Rita Traversi[4,6], Kitack Lee[3], Tuomo Nieminen[1,7], Lisa J. Beck[1], Markku Kulmala[1], Veli-Matti Kerminen[1] and Mikko Sipilä[1]

[1]Institute for Atmospheric and Earth System Research (INAR) / Physics, University of Helsinki, 00560, Helsinki, Finland
[2]Department of Electronics and Nanoengineering, Aalto University, P.O. Box 11000, 00076 Aalto, Finland
[3]Division of Environmental Science and Engineering, Pohang University of Science and Technology, Pohang, South Korea
[4]Department of Chemistry "Ugo Shiff" - University of Florence - Via della Lastruccia, 3, 50019, Sesto Fiorentino, Florence, Italy.
[5]Departamento de Ecología y Gestión Costera, Instituto de Ciencias Marinas de Andalucía (ICMAN-CSIC), Puerto Real, 11510, Cádiz, Spain
[6]Institute of Polar Science, ISP-CNR , Via Torino, 155 , 30172 Venezia Mestre, Venice, Italy.
[7]Institute for Atmospheric and Earth System Research (INAR) / Forest Sciences, University of Helsinki.

Correspondence to: Marjan Marbouti (marjan.marbouti@helsinki.fi)

Abstract. We examined the relationships linking atmospheric in-situ data of gas phase methane sulfonic acid (CH_3SO_3H, MSA), sulfuric acid (H_2SO_4, SA), iodic acid (HIO_3), highly oxidized organic molecules (HOM) and aerosol particle concentrations in the size ranges of 10–50 nm and 100–450 nm with satellite-derived chlorophyll a (Chl-a) and oceanic primary production (PP) during two time spans – the phytoplankton early bloom period, April-May 2017 (30 March–1 June, springtime) and phytoplankton late bloom; June–July 2017 (2 June–4 August, summertime) – in two ocean domains; Greenland Sea and Barents Sea. Atmospheric data were collected at Ny-Ålesund site in Svalbard, Norway. In general, Chl-a and PP in the Barents Sea were higher than in the Greenland Sea during the April–May period, whereas the Greenland Sea had higher Chl-a and PP during June–July. Phytoplankton bloom started by the loss of sea ice coverage in the Barents Sea at the marginal ice zone (MIZ) during April–May, and in the Greenland Sea close to Svalbard Island during June–July.

From the April–May period to the June–July period, the correlation between the ocean color data (Chl-a and PP) and MSA decreased in the Barents Sea and increased in the Greenland Sea, which establishes a direct relationship between the sea ice melting, phytoplankton bloom and atmospheric vapour composition. Both MSA and SA concentrations increased strongly during the bloom period, suggesting marine phytoplankton metabolism and resulting dimethyl sulphide (DMS) as the primary source of both MSA and SA in the Arctic atmosphere during spring–summer time. The highest correlation among all the atmospheric components and ocean color properties was observed between HIO_3 and Chl-a in both ocean domains during the springtime, but this feature may be connected to processes associated with the melting of sea ice. HOMs showed a low correlation with Chl-a and PP in comparison to other atmospheric vapours. The plausible explanation for such low correlation is that the primary source of volatile organic compounds (VOC) – precursors of HOM – is the soil or terrestrial vegetation of Svalbard archipelago rather than the ocean.

35   In springtime, small-particles (10-50 nm) correlated strongly with Chl-a in the Barents Sea and with PP in both oceanic domains, suggesting that biogenic productivity has a strong impact on new particle formation (NPF) in the springtime. In the summertime, small-particle concentrations showed almost no correlation with biogenic parameters, indicating that compounds not connected with phytoplankton metabolism, such as HOMs, have a critical role in summertime NPF. Larger particles (100–450 nm) showed an anti-correlation with Chl-a and PP in springtime, probably due to dilution of anthropogenic air pollution

40   (arctic haze) during spring. In the end of the Arctic haze period in April, particle-phase SA (non-sea-salt sulphate, $nss - SO_4^{2-}$) and particle phase MSA (MS$^-$) showed almost no correlation, whereas a connection between the gas phase MSA and SA concentrations was found. The likely reason for this is the same origin for gas phase MSA and SA (DMS oxidation), whereas SA in particle phase mostly originated from a long-distance continental source.

45   **1 Introduction**

Atmospheric new particle formation (NPF) influences the climate system by contributing to cloud condensation nuclei (CCN) concentrations, thereby impacting many cloud properties and Earth's radiation budget (e.g. Boucher et al. 2013; Gordon et al., 2017). The total particle number concentration in marine background conditions is very likely to be dominated by sea salt particles and those originating from NPF, especially in pristine regions such as the Arctic atmosphere (Dall'Osto et al., 2017,

50   2018, 2019; Croft et al., 2016).

The detailed NPF mechanisms and chemical compounds contributing to NPF in the high Arctic were resolved only recently. Sipilä et al. (2016) conducted studies at the Atlantic coasts of Ireland and Northern Greenland, next to sea ice. There, NPF was shown to proceed via homogeneous nucleation and subsequent condensation of iodic acid (HIO$_3$). Their results on the mechanism and dominant role of HIO$_3$ in NPF were confirmed by Baccarini et al. (2020) over the Arctic sea ice, as well as in

55   a CERN-CLOUD laboratory study by He et al. (2021) where, besides iodic acid, also iodous acid (HIO$_2$) was shown to play a role in especially neutral NPF. While iodine-based compounds seem to be responsible for NPF over the sea ice, NPF taking place over and in the vicinity of open arctic ocean was shown to proceed by ion-induced nucleation of sulfuric acid (H$_2$SO$_4$) and ammonia (NH$_3$), followed by condensation of H$_2$SO$_4$ (SA) and methane sulfonic acid (CH$_3$SO$_3$H, MSA) in springtime and also of highly oxidized organic molecules (HOM) in summertime (Beck et al., 2021). Ion-induced H$_2$SO$_4$ – NH$_3$ – nucleation,

60   experimentally studied also in CERN CLOUD chamber (Kirkby et al., 2011), was found to be responsible for initial NPF at coastal Antarctica as well (Jokinen et al., 2018).

Clearly, there are many precursor compounds for NPF and particle growth in the atmosphere – at least H$_2$SO$_4$, MSA, HOMs, NH$_3$ and HIO$_3$. Dimethyl sulfide (DMS), released upon bacterial catabolism of dimethylsulfoniopropionate (DMSP) produced by pelagic phytoplankton, is the most abundant form of sulfur compound released into the atmosphere from the ocean (Stefels

65   et al., 2007), and it may influence the radiative balance of the Earth (Bates et al., 1987; Simo, 2001). The potential role of marine DMS in regulating the climate system was introduced by Charlson et al. (1987), and reassessed and questioned by

many other follow-up studies (e.g. Quinn and Bates 2011; Green and Hatton., 2014). They highlighted that atmospheric DMS is rapidly oxidized by hydroxyl radicals and is then transformed into SA and MSA, both of which may contribute to the formation of new particles and CCN (Jang et al., 2016).

70 HOMs have been shown to have a major role in new particle growth over (vegetated) continents (Ehn et al., 2012, 2014; Bianchi et al., 2019), whereas both Antarctic and northern Greenland atmosphere are virtually HOM-free locations (Jokinen et al., 2018; Sipilä et al., 2016; Beck et al., 2021). In contrast to Antarctica and northern Greenland, high concentrations of HOMs - up to $\sim 10^8$ molecules/cm^3, values comparable to those observed in a boreal forest (Ehn et al., 2014), were recently reported in the summertime Ny-Ålesund atmosphere at the coast of Svalbard archipelago (Beck et al., 2021). Laboratory

75 studies have revealed that HOMs can play a critical role even in initial steps of NPF due to their low vapor pressures (Kirkby et al., 2016; Tröstl et al., 2016). The main source of HOMs is the oxidation of terpenes – biogenically emitted volatile organic compounds. Terpene oxidation is initiated by their reaction with ozone or hydroxyl radicals, followed by an auto-oxidation process that rapidly leads to high levels of oxygenation and low vapour pressures of the reaction products (Ehn et al., 2014).

It is known that oxidized iodine species, especially HIO$_3$, can initiate NPF (Sipilä et al., 2016; Baccarini et al., 2020), but the

80 sources of these compounds into the Arctic atmosphere remain unclear (Mahajan et al., 2010; Allan et al., 2015). Coastal areas are known as the most productive areas of iodine species, with iodine released from seaweeds exposed to ambient air during low tides (O'Dowd et al., 2002). However, also open ocean environments, as well as the Arctic and Antarctic sea ice, are sources of iodine-containing compounds (Atkinson et al., 2012). In a sea-ice region, marine phytoplankton and sea-ice algae, especially diatoms trapped within brine channels of sea ice, seem to be responsible for the production of iodine compounds

85 released to the atmosphere, depending on porosity of sea ice (Moore et al., 1996; Atkinson et al., 2012; Saiz-Lopez et al., 2015). Emitted iodine compounds, such as I$_2$, are photolabile and under solar radiation rapidly dissociate, forming highly reactive I radicals. These I radicals react promptly with ozone, resulting in the production of iodine oxides as well as iodous and iodic acids. Though HIO$_3$ nucleation, potentially assisted by HIO$_2$ (He et al., 2021) forms new particles close to sea ice (Sipilä et al., 2016; Baccarini et al., 2020; Beck et al., 2021), it remains unclear whether NPF initiated by HIO$_3$ or other iodine

90 species is important in remote open and ice-free ocean regions, and whether this phenomenon has a relevant contribution to the atmospheric aerosol and CCN populations.

In previous studies, the variability of gas phase DMS mixing ratio and particle phase MSA measured in-situ at Svalbard have been evaluated together with ocean color properties in surface waters in the vicinity of Svalbard during phytoplankton bloom periods, and a high correlation was found between atmospheric DMS and chlorophyll a (Chl-a) (Park et al., 2013; 2017; 2018).

95 Also, several studies have been performed to understand the relation between the particle phase MSA concentration and the parameters related to biogenic production (Chl-a and sea ice extent) from present-day observations in both hemispheres (e.g. Sharma et al., 2012; Becagli et al., 2013, 2016, 2019). However, connections of ocean color properties with both gas phase MSA, SA, HOMs and HIO$_3$ concentrations and atmospheric aerosol particle concentrations have not been investigated previously. These connections will be thoroughly examined in the present study. Another novelty of this work is the application

100 of merged satellite data. While previous studies used only Moderate Resolution Imaging Spectroradiometer (MODIS) data,

Atmospheric
Chemistry
and Physics
Discussions

Open Access
EGU

here we apply the OC-CCI data base containing merged products (SeaWiFS, MODIS, VIIRS) with a better data quality and larger coverage. There are no studies that evaluate primary production (PP) in connection with atmospheric components (MSA, SA, HIO$_3$, HOM and aerosol particle concentrations). The only study addressing the role of PP in production of above discussed compounds is focusing on particle phase MSA (Becagli et al., 2016).

105 In this study, we combine in-situ field measurements of gas phase SA, MSA, HOMs and HIO$_3$ concentrations and aerosol particle concentrations in the size ranges of 10–50 nm and 100–450 nm performed in Ny-Ålesund, Svalbard, with satellite measurements of Chl-a, PP (calculated by a bio-optical, physiologically based, semi-analytical model) and sea ice extent during April–May, 2017 (30 March–1 June) and June–July, 2017 (2 June–4 August) in two ocean domains, Greenland Sea and Barents Sea. We aim to understand and investigate the roles of Chl-a, PP and sea ice extent in controlling and producing the in-situ

110 measured MSA, SA, HIO$_3$, HOM and aerosol concentrations over the Greenland and Barents Seas. We also investigated the behaviour of gas phase and particle phase MSA and SA.

2. Methodology

2.1 Sampling sites

Field measurements were performed at Gruvebadet laboratory in Ny-Ålesund (78.9° N, 11.9° E), ca. 1.5 km south from the

115 main village (Fig. 1). A trajectory analysis was performed to identify the primary source areas of atmospheric vapours and aerosol particles sampled at the site. Based on the trajectory analysis, we divided source areas into three sectors (Fig. 1): the Barents Sea (70° N–78.92° N; 11.89° E–60° E), the Greenland Sea (70° N–78.92° N; 40° W–11.89° E), and sea ice area (78.92° N–90° N; 40° W–60° E). These sectors had 28%, 25% and 46% (13% from east of Ny-Ålesund sea ice and 33% from west of Ny-Ålesund sea ice) contributions to the air mass origins, respectively. The sea ice sector was largely dominant, but

120 because it is not possible to measure beneath the sea ice, our approach could be used to study this area (sea ice algae). Simultaneous particle-phase MSA and SA measurements, performed at the same site, were adopted from a previously published study by Becagli et al. (2019). Satellite data from Greenland and Barents Seas were retrieved for quantification of PP and Chl-a concentration which connections to in-situ recorded variables will be evaluated in this study.
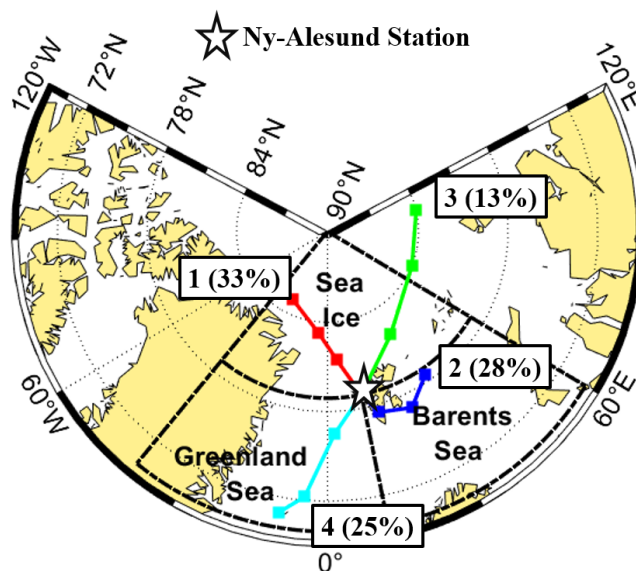
Figure 1. A map of the Arctic region around the sampling site. The three main source regions for airmasses reaching Ny-Ålesund are defined with black dashed lines and mean trajectories of each trajectory cluster reaching Ny-Ålesund from 30th March to 4th August 2017 are displayed.

2.2 Sampling methods and chemical analysis

Gas phase MSA, SA, HIO_3 and HOMs concentrations were measured with a nitrate ion Chemical Ionization – Atmospheric Pressure interface - Time-of-Flight - mass spectrometer (CI-APi-TOF) described in Jokinen et al. (2012). The CI-APi-TOF has been used in numerous previous field and laboratory studies, including those used to reveal detailed mechanisms of the Arctic and Antarctic NPF (Sipilä et al., 2016; Jokinen et al., 2018; Baccarini et al., 2020; Beck et al., 2021). Shortly, the operation is based on proton transfer between the reagent ion (NO_3^-) and sample constituents (for SA, MSA, HIO_3), or on adduct formation of sample molecule and the reagent ion (in case of HOM). Ionized sample is drawn via atmospheric pressure interface, comprised of quadrupoles and ion lenses, to a time-of-flight chamber where ions are mass/charge separated and eventually detected by a micro-channel plate detector. The mass spectra were analyzed with the Matlab-based software package tofTools developed by Junninen et al. (2010). In this work, HOM refers to sum concentration of all detected, highly oxidized species with molecular masses between 300 and 600 Da. Exact identification of all (more than 100) individual HOM compounds remains a topic for a further study. The particle number size distribution was measured with a SMPS in the size range of 10 to 450 nm (Xue et al., 2015).

The particle-phase methane sulphonate ($CH_3O_3S^-$, MS^-) concentration, representing condensed MSA, and non-sea salt sulphate (nss-SO_4^{2-}) concentration, representing condensed SA, as well as sulphate formed in the liquid phase, were measured by ion

Atmospheric
Chemistry
and Physics
Discussions

chromatography on the aqueous extract of aerosol collected on Teflon filter. The aerosol sampling and analytical procedures have been reported in detail by Becagli et al. (2016).

2.3 Satellite ocean color data (Chl-a and PP)

Eight-day (8D) average of Chl-a were downloaded from the OC-CCI website (http://www.esa-oceancolour-cci.org) with a spatial resolution of 4 km. The OC-CCI is a long-term, consistent and error-characterized dataset generated from merged normalized remote-sensing reflectance derived from four satellite sensors: SeaWiFS, MODIS, MERIS, and VIIRS (Plummer et al., 2017). In this work we used OC-CCI v3.0. Primary Production data (8D) which were downloaded from http://www.science.oregonstate.edu/ocean.productivity/index.php. The time series were computed in the two selected domains by spatially averaging the 4-km, 8-day data sets. Missing values in the Arctic regions are mainly due to either cloudiness or algorithm failure. However, overall, there are enough cloud-free data to describe the evolution of Chl-a and PP for our sampling site. We did not go through sea ice analysis deeply in this research, but daily sea ice extent (SIE) was added to find melting time for phytoplankton bloom. SIE data were obtained from the EUMETSAT OSI SAF. This data product was daily and titled 'SSMIS Sea Ice Concentration Maps on 10 km Polar Stereographic Grid' in 10 km resolution. The daily SIE data are averaged over each month. We also utilized sea ice extents images from the National Snow and Ice Data Center (NSIDC) https://nsidc.org/ to look at sea ice extent area in the Barents and the Greenland Seas.

2.4 Trajectories map

Three-dimensional, three-day (72 h) back trajectories were calculated using the Hybrid Single-Particle Lagrangian Integrated Trajectory (HYSPLIT) model from the National Oceanic and Atmospheric Administration Air Resources Laboratory (Draxler and Hess, 1998) (Fig. 1). The calculations are based on meteorological data from the NCEP's (National Weather Service's National Centres for Environmental Prediction) Global Data Assimilation System (at $1 \times 1°$ spatial resolution). Each trajectory consists of 72 endpoints, one per hour. Air masses were modelled to arrive at the altitude of 50 m above sea level (a.s.l.) at the coordinates of the research station for every hour of the campaign period.

Calculated back trajectories of air masses were grouped into trajectory clusters to see when air masses were arriving from the different sectors. Cluster analysis is a technique to separate a large data set into groups with similar properties. The k-means clustering algorithm was used. This function divides a data set into a specified number of groups, so that observations within a group are closely related to each other and each group has the least possible similarities to the other groups. The clustering analysis was carried out based on Euclidean distances between trajectories. Initially, each trajectory is defined to be a cluster. For the first iteration, two trajectories are paired. For every combination of trajectory pairs, the cluster spatial variance, which is the sum of squared distance between the endpoints of cluster's component trajectories, is calculated. Then, the total spatial variance (TSV), the sum of all the cluster spatial variance over all clusters, is calculated. The pair of clusters finally combined are the ones with the smallest change in TSV. The iterations continue until the last two clusters are combined. The percent change in TSV and number of clusters for each iteration are recorded. The final cluster number was determined by the point

175 of inflexion on the curve of percent change in TSV vs. number of clusters. More details about this methodology can be found in Stein et al. (2015).

We also counted how many hours air masses had spent over different surfaces on their way to the Gruvebadet station during the 72 hours prior to their arrival at the site. Three different surfaces were considered: open ocean (ocean with less than 15% sea-ice cover), sea-ice (more than 15% sea ice), and land. The influence of the surface types on the measured gas-phase and

180 aerosol concentrations were examined by correlating the concentrations with the time over certain surface type related to the air mass arriving at the time of each concentration measurement. The correlations were examined in 5-hour bins.

3 Result and discussion

3.1 Seasonal evolution of atmospheric components (MSA, SA, HIO₃, HOM) and aerosol concentration (10-50 nm, 100-450 nm) at Ny-Ålesund

185 **3.1.1 Comparison of gas-phase (MSA and SA) and particle-phase (MS⁻ and $nss - SO_4^{2-}$) composition**

MSA at Ny-Ålesund shows a seasonal pattern, with a steeply increasing concentration in April and May and decay toward a background concentration starting in early June (Fig. 2a). A similar seasonal pattern was observed for the particle-phase methane sulphonate sampled at the same site (Becagli et al., 2019) (Fig. 2b). However, in July MSA and MS⁻ in the particle-phase show a different pattern with very high values of MS⁻ respect to MSA. The increase of the MS⁻/MSA ratio of about 38

190 in April–May up to 330 at mid-July (Fig. 3) can be due to three different reasons. First, the different gas-to-particle conversion rate that is lower in April–May compared to July, leading to a higher MSA/MS⁻ ratio in April–May than in July. The repartitioning between the gas and particulate phases could be one of the causes of the different slope of the linear regression in spring (April–May) and in summer (June–July). Second, the dominant oxidation pathway of DMS, i.e. gas or liquid phase oxidation, could change between spring and summer. Third, the oceanic source area of DMS in July is more distant than in

195 April-May, giving more time to the formation of MS⁻ in aerosol phase. Conversely, SA in the gas phase and non-sea salt sulphate ($nss - SO_4^{2-}$) in the particle phase show completely different trends (Fig. 2c,d), especially during April (Fig. 4a,b). This is due to the dominant anthropogenic source of $nss - SO_4^{2-}$ in the particulate matter during the Arctic Haze period (e.g. Quinn et al, 2007).
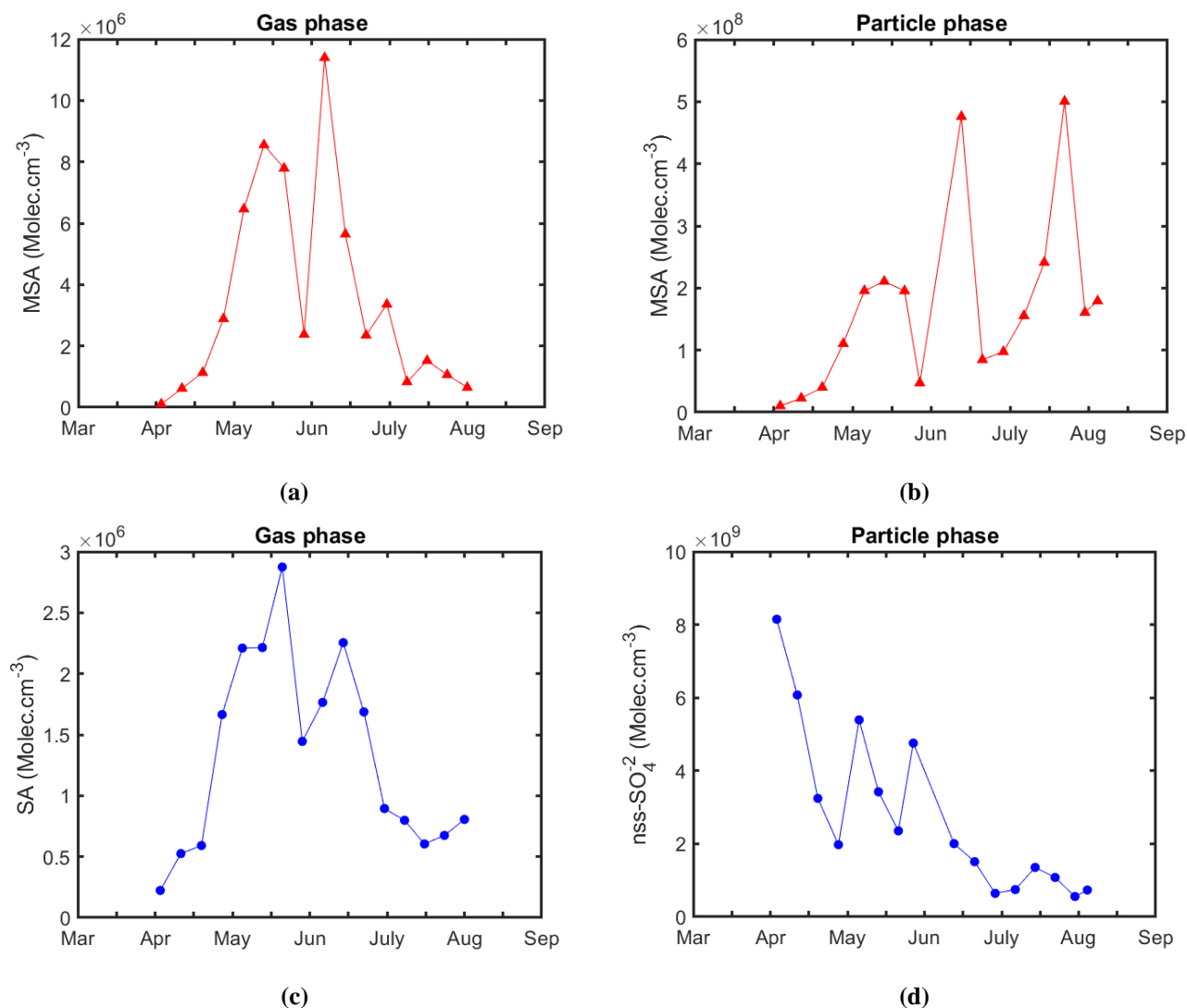
Figure 2. Time evolution of (a) MSA concentration – gas phase (b) MSA concentration – particle phase (MS^-, $CH_3O_3S^-$) (c) SA concentration – gas phase (H_2SO_4) and (d) $nss - SO_4^{2-}$ – particle phase measured on 31st March – 4th August 2017 at Ny-Ålesund. Particle phase measurements are adopted from Becagli et al. (2019).
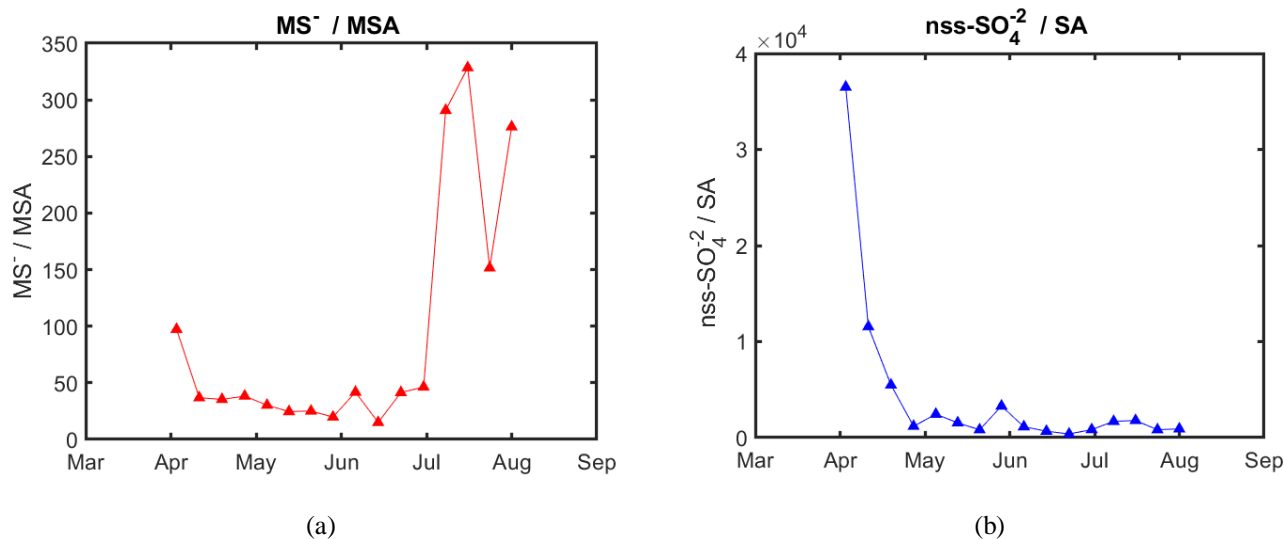
Figure 3. (a) MS⁻/MSA (b) $nss - SO_4^{2-}$ /SA ratio during the period of study.

205

During the Arctic haze period, a strong correlation is observed between gas-phase MSA and SA (R^2=0.91, Fig. 4c), whereas particle phase MS⁻ and non-sea salt sulphate seem not to be correlated (R^2=0.19, Fig. 4d). The good correlation between MSA and SA concentrations points toward the same origin, marine DMS, of these compounds. Gas phase MSA and MS⁻ originate solely from DMS oxidation, which could explain their similar temporal behaviour (Fig. 4a), whereas SO₂, the precursor of gas phase SA and particle-phase $nss - SO_4^{2-}$, originates from both DMS oxidation and anthropogenic sources. Since MSA and also largely SA originate from DMS oxidation, it is natural that their temporal evolution follows similar patterns as the atmospheric DMS mixing ratio described by several ocean color data. A previous study regarding sulfate stable isotope analysis showed that more than 60% of sulfate aerosol in the Arctic is of anthropogenic origin (Li et al., 1993b). However, unlike sulfuric acid (H₂SO₄), anthropogenic sulfate aerosol can be transported long distances and sulphate can be formed also in aqueous phase during cloud processes. Thus, particle phase sulphate ($nss - SO_4^{2-}$) shows completely different temporal and spatial variation compared with MSA, MS⁻ and SA, with maximum concentrations (Fig. 4a,c) observed during the Arctic haze period (e.g. Quinn et al 2007).
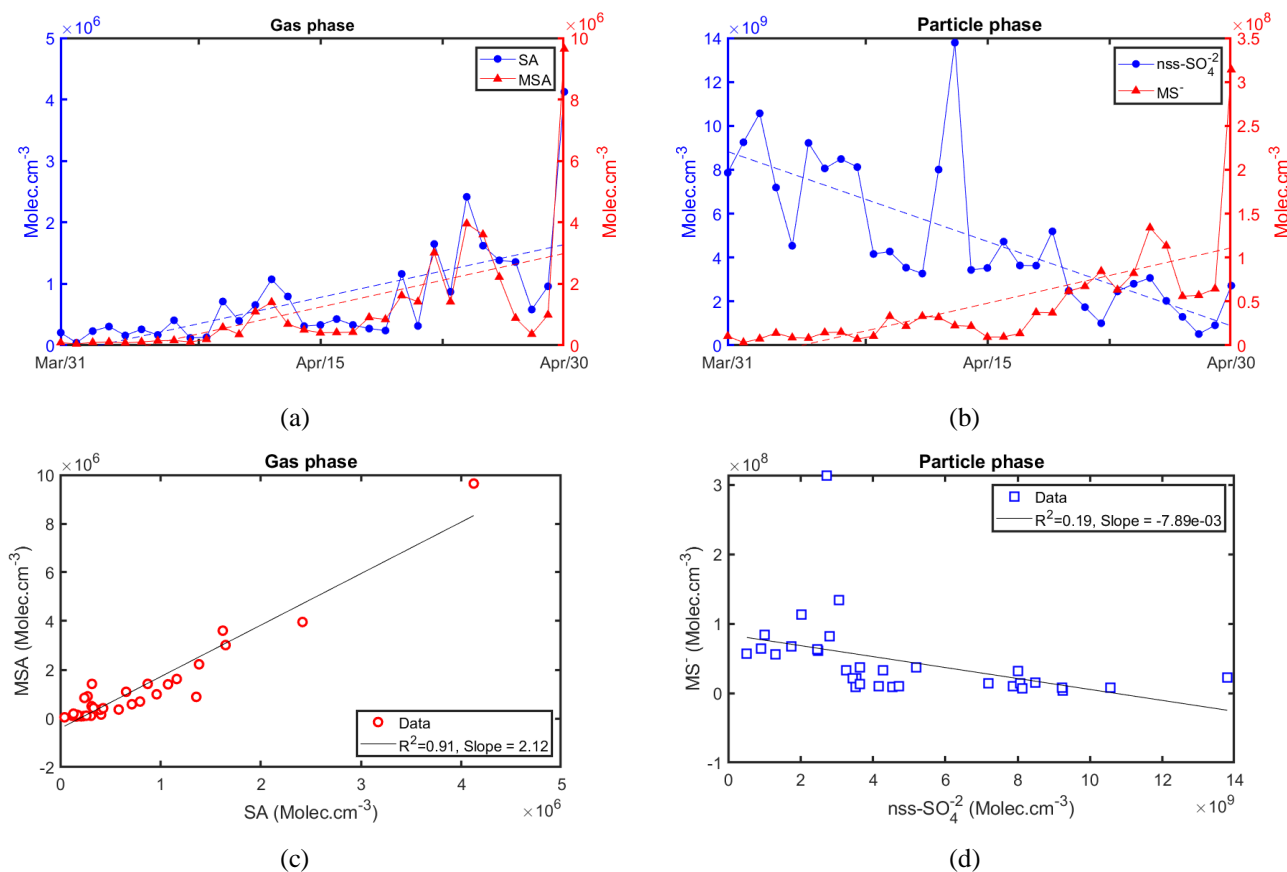
Figure 4. (a) Vapour concentrations of SA (H_2SO_4) and MSA, by increasing DMS emissions and radiation. (b) Particle phase concentrations of $nss-SO_4^{2-}$ and MS^- characterized by the decay of residuals of the Arctic haze (c) The relationship between SA and MSA measured at Ny-Ålesund. (d) The relationship between particle phase $nss-SO_4^{2-}$ and MS^- measured by Becagli et al. (2019) in April 2017.

It is noteworthy that the pathways of DMS oxidation to SA (via SO_2) or MSA, and their relative yields, are controlled by many environmental factors, such as the temperature, solar irradiance and concentrations of HO_x and NO_3 radicals as well as NO_x and BrO (Read et al., 2008). Especially, more MSA is produced as the temperature decreases (Hynes et al., 1986). Therefore, the kinetics of the chemical oxidation process should be resolved in detail before the reasons for the variation of MSA/SA - ratio can be fully explained. Besides the decay of phytoplankton productivity and boundary layer dynamics, also precipitation scavenging could be a reason for decreasing concentrations of MSA and SA during summer (Li et al., 1993a).

MSA and SA followed typical seasonal variation, which is wide-spread in northern high latitudes (Li et al., 1993b). It is also known that there is a significant fluctuation in concentration from early spring to late summer for these sulfur compounds (Li et al., 1993b). At the Ny-Ålesund region, SA, assisted by NH_3 and air ionization, is the driver and initiator of NPF. Because of its relatively high vapour pressure compared with SA, MSA condenses primarily onto pre-existing particles, even though

its contribution to initial cluster formation has not been excluded e.g. in upper atmospheric layers (Beck et al., 2021). If relative

235 yields of SA and MSA are changed due changes in an atmospheric environment, that could be reflected in the formation rates of new particles.

3.1.2 Temporal evolution of gas phase HIO₃ and HOM

HIO_3 concentrations also peak in mid-May (Fig. 5a). However, both the springtime increase and summertime decrease are less pronounced compared with MSA and SA. Sipilä et al. (2016) and Beck et al. (2021) reported a steep increase of the HIO_3

240 concentration – from 10^5 cm^{-3} up to 10^7 - 10^8 cm^{-3} levels – after the end of polar night at the Villum Research Station (Station Nord) in Northernmost Greenland. Concentrations decayed back to low levels during summer. Since Station Nord is surrounded by the sea ice throughout the year, Sipilä et al. (2016) speculated that the source of the iodine that produces HIO_3 would be the sea ice. Nevertheless, at Ny-Ålesund both the steepness of increase and the concentration of HIO_3 are much lower (Beck et al. (2021).

245 Out of all studied vapours, HOMs show completely different temporal behaviour as reported in an earlier study (Beck et al., 2021). Their concentrations start to increase in the middle of May when all other studied compounds start to decay (Fig. 5b). This is an indication that HOM may have completely different sources than MSA, SA and HIO_3. The start of the HOM concentration increase coincides with the snow melt and exposure of soil and tundra vegetation, which could be speculated to release sufficient amounts of VOCs to be oxidized to form HOMs.


(a)   (b)
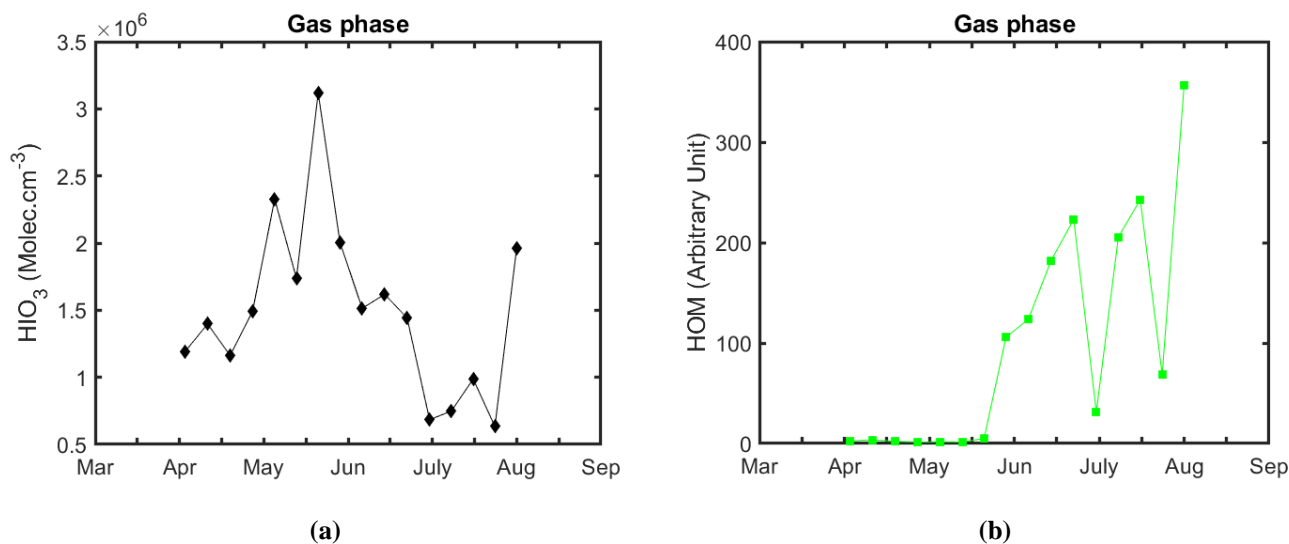
250 **Figure 5.** Time evolution of gas phase (a) HIO₃ concentration and (b) HOM concentration measured between 31st March and 4th August 2017 at Ny-Ålesund.

3.1.3 Temporal evolution of aerosol concentrations

Aerosol particle number concentrations were analyzed in two size ranges, 10–50 nm and 100–450 nm (Fig. 6). Particles in the

255   10–50 nm size range are indicative of NPF and growth, whereas the larger accumulation mode particles in the 100-450 nm

size range represent more aged particles. Concentrations of 10–50 nm particles have an increasing pattern from the beginning

of our measurements (1 April), whereas concentrations of 100–450 nm particles have a decreasing pattern. The smaller

particles (10–50 nm) are likely enhanced by biogenically originated gases, SA and MSA, whereas the larger particles are much

more related to the presence of Arctic Haze (Park et al., 2017). Therefore, the number concentration of 100–450 nm particles

260   showed a decreasing pattern as Arctic Haze decayed.
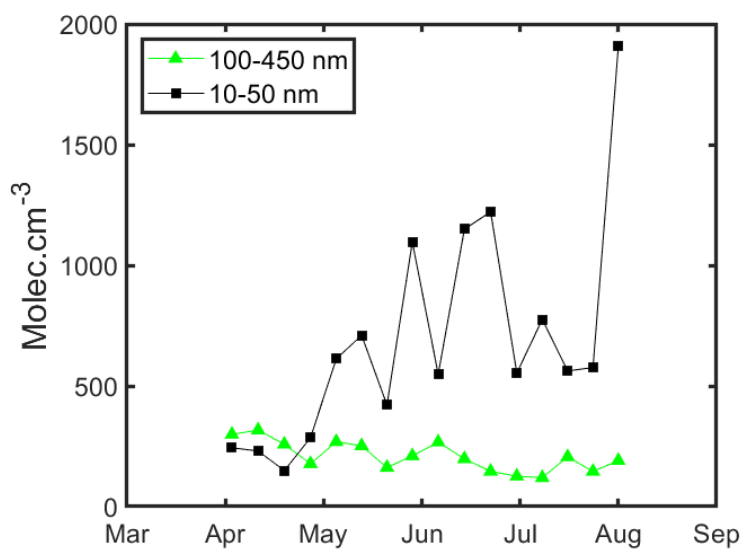
Figure 6. Time evolution of 10-50 nm and 100-450 nm aerosol particle concentrations measured at Ny-Ålesund.

3.2 Ocean colour time series affected by the Barents and the Greenland Seas and sea ice properties

265   During April and May 2017, the Chl-a concentration in the Barents Sea was about 50% higher than that in the Greenland Sea.

After that, the pattern changed and during summer, Chl-a concentration in the Greenland Sea exceeded that in the Barents Sea

(Fig. 7a). A likely reason for this could be an earlier phytoplankton bloom in the Barents Sea, possibly due to earlier sea ice

melting (Fig. 8). The Barents Sea is characterized by an early phytoplankton bloom, as revealed by Wassmann et al. (2006a),

starting in April at the marginal ice zone (MIZ). The early blooms were triggered by the stratification induced by the melting

270   ice (Matrai et al., 2007). This kind of bloom is usually dominated by the prymnesiophyceae (Rat'kova and Wassmann, 2002;

Matrai et al., 2007), together with diatoms. Furthermore, high grazing rates were generally found (Wassmann et al., 2006b),

which promote high DMS emissions. Nevertheless, the blooms are transient local events due to quick nutrient consumption, and are not propagating over the whole region (Perrette et al., 2011).
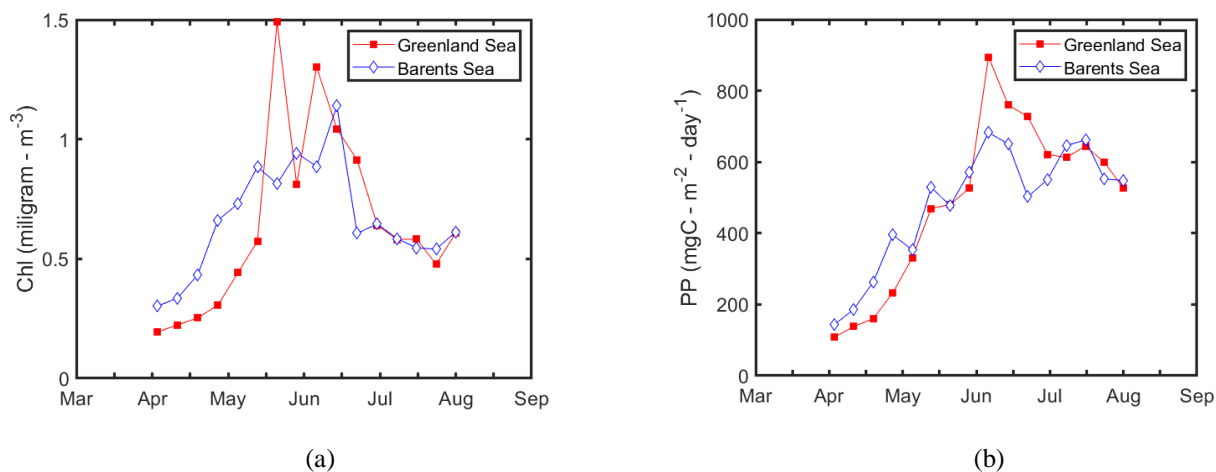

Figure 7. Four-month evolution of (a) Chl-a and (b) PP, calculated for the Barents Sea and Greenland Sea. All data are calculated as 8-day averages.

PP was higher in the Barents Sea compared with the Greenland Sea during April and May, whereas during summer PP was higher in the Greenland Sea (Fig. 7b). Such behaviour of PP can be explained by the earlier ice melting (Fig. 8) and plankton bloom in Barents Sea, similar to the behaviour of Chl-a. As already observed in the Greenland Sea, sea ice extent presents the main decrease during the June–July period, likely corresponding to the maximum values of Chl-a and PP in summer, but a slight decrease in sea ice extent started already in April that can promote the slight increases of Chl-a and PP already in April. Therefore, the different timing of sea ice melting in Greenland Sea causes the shape of spring-summer Chl-a and PP peaks.
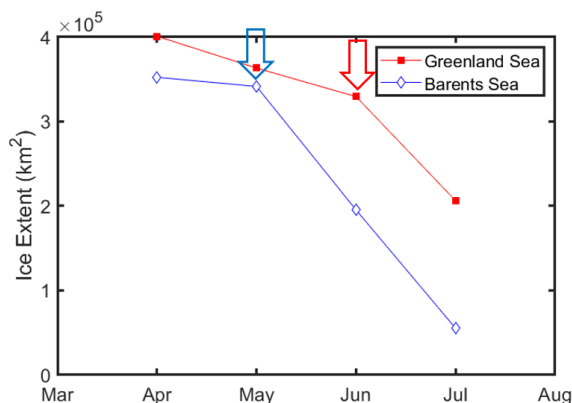

Figure 8. Monthly sea ice extent during April – July 2017. Red and blue arrows indicate the starting of massive sea ice melting in Barents and Greenland seas respectively.

285

3.3. Correlation between biologic parameters (Chl-a and PP) and atmospheric components (MSA, SA, HIO$_3$, HOM and aerosol concentrations) in April-May (phytoplankton bloom time) and June-July 2017 (post - phytoplankton bloom time).

Atmospheric measurements were conducted from the end of March until the beginning of August. This period was divided
290 into two parts: the bloom time (April–May) and the post-bloom time (June–July). Key ocean color factors that influence the atmospheric concentrations observed in-situ at Ny-Ålesund were identified. The back-trajectory cluster analysis revealed that at least some of the atmospheric components observed at Ny-Ålesund originate from two different source areas, the Barents Sea and the Greenland Sea, both in spring (April–May) and summertime (June–July). Figures A1–A6 show the scatter plots between atmospheric concentrations and ocean color parameters.

295 **3.3.1 Biologic parameters (Chl-a and PP) and MSA during April–May and June–July, 2017**

Table 1 shows that MSA concentrations measured at Ny-Ålesund correlated well with Chl-a and PP in the Greenland Sea and Barents Sea. This suggests, as expected, that MSA formation is strongly related to biomass concentration and productivity in these two oceanic areas, with a higher influence of the Barents Sea during the springtime (April–May) and the Greenland Sea in the summertime (June–July).

300 As mentioned before, sea ice melting in the Barents Sea starts before that in the Greenland Sea (Fig. 8), so that the Barents Sea is characterized by an early phytoplankton bloom due to sea ice melting in the "bloom-dominated regime". Therefore, a strong correlation between MSA and Chl-a in the Barents Sea was found during April–May ($R^2=0.56$) while the correlation during June–July was somewhat weaker ($R^2=0.49$). Sea ice melting in the Greenland Sea starts later, around June, so the correlation between MSA and Chl-a in the Greenland Sea increased from 0.4 during April–May to 0.83 during June–July.
305 Figure 8 shows that the sea ice extent was reasonably constant in the Svalbard side of the Greenland Sea until about July. PP followed similar patterns in two ocean domains, but had maximum values in different times.

**3.3.2 Biologic parameters (Chl-a, PP) and SA during April–May and June–July, 2017**

In the gas phase and in the absence of anthropogenic SO$_2$ pollution, MSA and SA have the same origin: DMS oxidation to MSA and SO$_2$ with subsequent oxidation of SO$_2$ to SA. Therefore, a high correlations between SA and ocean color parameters
310 were found here as well (Table 1, Fig. A2). SA also has a similar pattern as MSA during the spring and summer times, with some differences both in the slope and significance of the correlation. Such differences could be due to the differences in the yield of MSA with respect to SA from DMS oxidation. Figure 9 shows the relation between the MSA/SA ratio and radiation intensity. The MSA formation is favoured with respect to SA especially in summer when radiation is at its strongest.
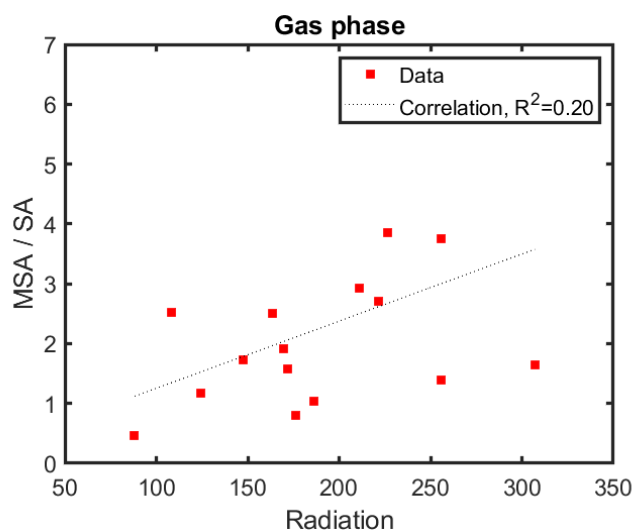
Figure 9. Temporal development of MSA/SA-ratio and UV radiation at Ny-Ålesund.

3.3.3 Biologic parameters (Chl-a, PP) and HIO₃ during April-May and June-July 2017

During the springtime, the HIO_3 concentration has strong correlations with the ocean color parameters (Chl-a and PP) in the Greenland Sea (Chl-a: $R^2=0.82$, PP: $R^2= 0.55$) (Table 1, Fig. A3). These correlations decreased during the summertime. The reason for such behaviour could be that HIO_3 observed in Ny-Ålesund results from the sea ice-emitted iodine. Ice-borne phytoplankton bloom is likely to be intense during spring (Sipilä et al., 2016) but decays away by summer. Thus, the high springtime correlation and low summertime correlation may just be a coincidence and there is no causal connection between open ocean properties and observed HIO_3 concentrations. The production and release of iodine from the sea ice likely depends on the ice thickness that determines the fraction of solar radiation penetrating through and available for phytoplankton photosynthesis, as well as on the amount of nutrients, ice porosity etc. The connection between HIO_3 and sea-ice is further supported by the strong increase in the measured HIO_3 concentration at Ny-Ålesund with an increasing time the arriving air mass had spent over sea-ice (Fig. 10). However, the exact details of ice-borne or under-ice plankton iodine production are currently not known. Also, other mechanisms, including pelagic phytoplankton activity, leading to iodine emissions may contribute to the observed iodic acid formation.
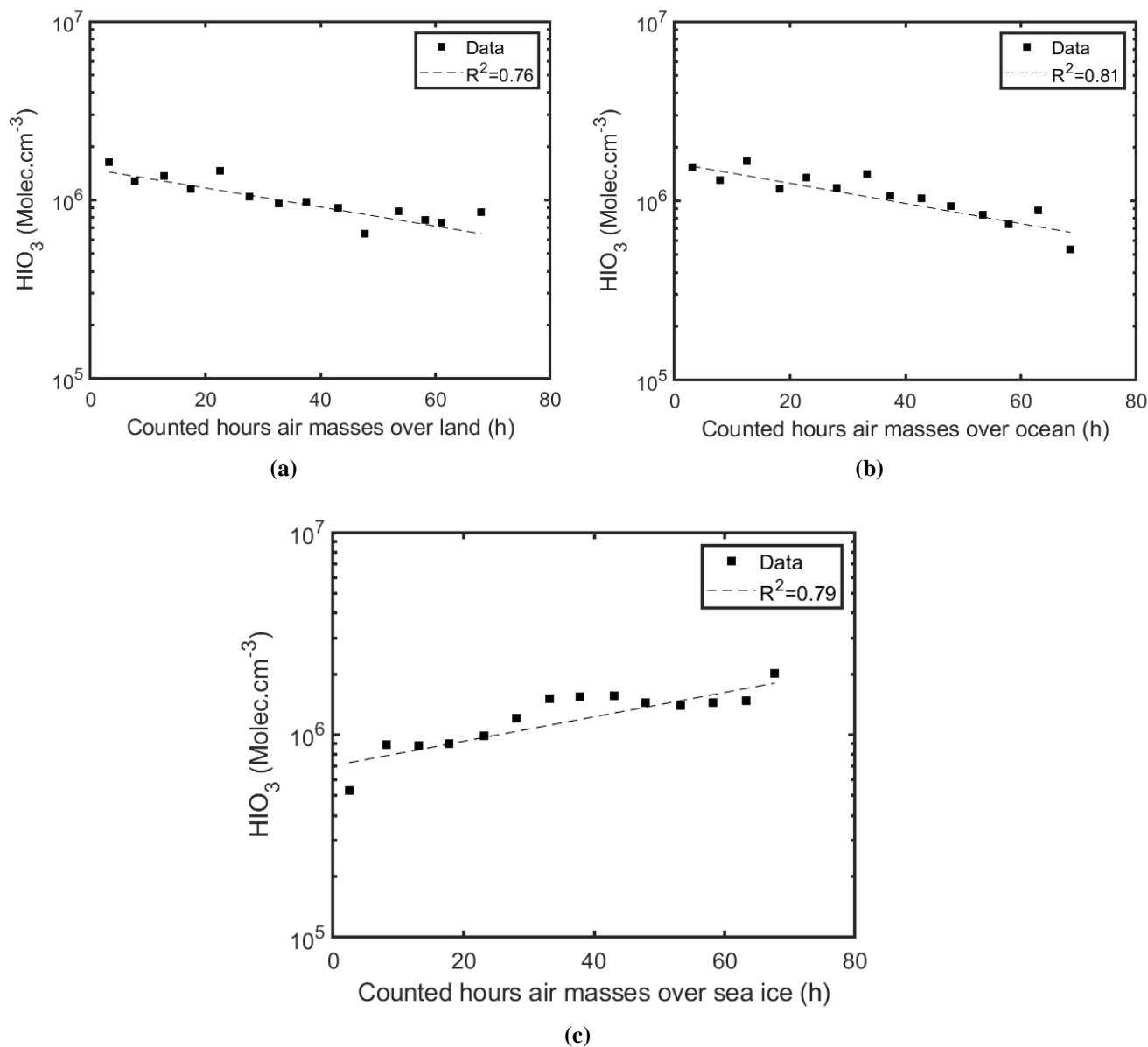
Figure 10. Concentration of HIO₃ as function of the time air mass has spent (a) over land; (b) over ocean; (c) over sea ice during the total duration (72 hours) of backward calculation.

3.3.4. Biological variables (Chl-a and PP) and HOM concentration during April–May and June–July, 2017

335 Based on Table 1 and Fig. A4, HOM is the only atmospheric constituent out of all the studied compounds, the correlation of which with Chl-a and PP was extremely low during both spring and summer for both oceanic regions. This indicates that HOMs probably have completely different sources than MSA, SA and HIO_3. Rather than pelagic plankton, observed HOM concentrations can be associated with VOC emissions from local terrestrial ecosystems or long-range transportation of VOCs or semi-volatile organic compounds (SVOC) from continental Eurasian regions emitting vast amounts of VOCs from boreal

340 forests. These VOCs or SVOCs would then be oxidized to form HOM nearby the measurement site. HOM itself cannot be long range transported due its short lifetime against condensational loss. HOM vapour pressures are so low that they tend to condense onto particles, some of them even irreversibly. The very steep and quite abrupt increase in the HOM concentration in the end of May would, however, suggest the VOC source to be the terrestrial vegetation or soil in Svalbard. That increase coincides with the snow melt and soil exposure (Beck et al., 2021). Also efficient VOC production in continental Europe starts

345 well before the end of May, and less sudden increase would be expected. Our observations support the suggestion by Beck et al. (2021) on the continental or local source of VOC acting as the main HOM precursor.

3.3.5. Biologic variables (Chl-a and PP) and aerosol particle concentrations (10-50 nm – small-particles and 100-450 nm – large-particles) during April-May and June-July 2017

Strong correlations between small-particle (10–50 nm) concentrations and ocean color parameters were found during the

350 springtime in the Barents Sea (Chl-a: R^2=0.68, PP: R^2=0.63) and in the Greenland Sea (PP: R^2=0.7), whereas correlations during summertime (June–July) were extremely low both in the Barents Sea (Chl-a: R^2=0.01, PP: R^2=0.16) and in the Greenland Sea (Chl-a:R^2=0, PP:R^2=0.1) (Table 1, Fig. A5). Strong springtime correlations suggest that biogenic (phytoplankton) productivity represent about the 65% of the small particle formation variability during this season, and that SA and/or MSA arising from biogenic productivity have an important role in NPF. In summertime, however, the small-particle

355 concentration does not correlate with SA, MSA, Chl-a and PP. Beyond SA and MSA, other vapours, such as HOM (Beck et al., 2021), are thus needed to explain the summertime occurrence of small- particles.

As shown in Table 1 and Fig. A6, the concentration of 100–450 nm particles anti-correlate with the ocean color data during springtime. The strengths (R^2 values) of these anti-correlations are 0.5 for Chl-a and 0.38 for PP in the Greenland Sea, and 0.45 and 0.51, respectively, in the Barents Sea (Table 1, Fig. A5). This is an expected feature, since larger particles represent

360 mostly anthropogenic pollution (Arctic haze) during early spring. When the polar vortex breaks up in the spring, the clean air flows to the Arctic and dilutes the pollution, resulting in the decreasing concentration of larger particles. Because of that, we cannot separate a possible signal from biogenic processes in the >100 nm aerosol particle population.

365

Ocean color-atmospheric data	Greenland (April - May)	Barents (April-May)	Greenland (June-July)	Barents (June-July)
Chl-a - MSA	$R^2 = 0.40$ $P = 9.01e-02$	$R^2 = 0.56$ $P = 3.29e-02$	$R^2 = 0.83$ $P = 1.63e-03$	$R^2 = 0.49$ $P = 5.18e-02$
PP - MSA	$R^2 = 0.55$ $P = 3.58e-02$	$R^2 = 0.46$ $P = 6.31e-02$	$R^2 = 0.83$ $P = 1.56e-03$	$R^2 = 0.27$ $P = 1.88e-01$
Chl-a and SA	$R^2 = 0.58$ $P = 2.86e-02$	$R^2 = 0.68$ $P = 1.13e-02$	$R^2 = 0.78$ $P = 3.73e-03$	$R^2 = 0.76$ $P = 5.04e-03$
PP and SA	$R^2 = 0.64$ $P = 1.73e-02$	$R^2 = 0.59$ $P = 2.62e-02$	$R^2 = 0.62$ $P = 2.04e-02$	$R^2 = 0.04$ $P = 6.42e-01$
Chl-a and HIO_3	$R^2 = 0.82$ $P = 1.94e-03$	$R^2 = 0.44$ $P = 7.14e-02$	$R^2 = 0.30$ $P = 1.61e-01$	$R^2 = 0.23$ $P = 2.25e-01$
PP and HIO_3	$R^2 = 0.55$ $P = 3.62e-02$	$R^2 = 0.35$ $P = 1.20e-01$	$R^2 = 0.07$ $P = 5.20e-01$	$R^2 = 0$ $P = 9.76e-01$
Chl-a and HOM	$R^2 = 0.08$ $P = 5.10e-01$	$R^2 = 0.24$ $P = 2.20e-01$	$R^2 = 0.01$ (anti-correlation) $P = 8.52e-01$	$R^2 = 0.01$ (anti-correlation) $P=8.07e-01$
PP and HOM	$R^2 = 0.28$ $P = 1.76e-01$	$R^2 = 0.28$ $P = 1.80e-01$	$R^2 = 0.08$ (anti-correlation) $P =5.07e-01$	$R^2 = 0$ (anti-correlation) $P = 9.98e-01$
Chla and (10-50 nm)	$R2 = 0.17$ $P = 3.08e-01$	$R^2 = 0.68$ $P = 1.15e-02$	$R^2 = 0$ (anti-correlation) $P = 9.83e-01$	$R^2 = 0.01$ $P = 8.34e-01$
PP and (10-50 nm)	$R^2 = 0.7$ $P = 9.62e-03$	$R^2 = 0.63$ $P = 1.84e-02$	$R^2 = 0.1$ (anti-correlation) $P = 4.34e-01$	$R^2 = 0.16$ (anti-correlation) $P = 3.22e-01$
Chla and (100-450 nm)	$R2 = 0.5$ (anti-corelation) $P = 5.05e-02$	$R^2 = 0.45$ (anti-corelation) $P = 6.70e-02$	$R^2 = 0.46$ $P = 6.39e-02$	$R^2 = 0.26$ $P = 1.96e-01$
PP and (100-450 nm)	$R^2 = 0.38$ (anti-corelation) $P = 1.05e-01$	$R^2 = 0.51$ (anti-corelation) $P = 4.52e-02$	$R^2 = 0.41$ $P = 8.93e-02$	$R^2 = 0.35$ $P = 1.24e-01$

Table 1. Correlation of atmospheric measurements (MSA, SA, HIO_3, HOM) and aerosol concentrations (10-50nm, 100-450nm) with ocean color parameters (Chl-a and PP) for Barents Sea and Greenland Sea in the period April-May and June-July at Ny-Ålesund.

370 **4 Summary and conclusions**

This study investigates the relationships among pelagic chlorophyll a (Chl-a) concentration and primary production (PP) in the Barents and the Greenland Seas, and gas phase concentrations of methanesulfonic acid (MSA), sulfuric acid (SA), iodic

Atmospheric
Chemistry
and Physics
Discussions

acid (HIO_3), highly oxidized organic molecules (HOM) and aerosol concentrations (size ranges of 10–50 nm and 100–450 nm) measured at Ny-Ålesund, Svalbard islands. Five months of in-situ measured data of atmospheric vapours and aerosol particles,

375   satellite-based measurements of Chl-a and sea ice distribution, and calculations of primary production at the potential source areas located in the surrounding oceanic regions (the Barents Sea and the Greenland Sea) were used in the analysis. Particle-phase measurements of MSA (methane sulphonate ($CH_3O_3S^-$) concentration, MS^-) and SA (non-sea salt sulphate (nss-SO_4^{2-}) concentration) from Becagli et al. (2019) were used as supporting data in this study.

380   The trajectory analysis shows that out of atmospheric vapours relevant for NPF and particle growth, SA and MSA originate primarily from the Barents Sea and Greenland Sea, depending on season and on the synoptic meteorological configuration. Other relevant vapours, HIO_3 and HOMs, unlikely originate from the open ocean phytoplankton activity while they still can be important for aerosol formation.

385   In the study by Becagli et al. (2019), the correlation between the particle-phase MSA (MS^-) and $nss-SO_4^{2-}$ concentrations was very low (R^2=0.19) due to difference sources of MSA (only oxidation of DMS) and $nss-SO_4^{2-}$(oxidation of DMS and anthropogenic sources - long-range transport). As Becagli et al. (2019) studied the composition of aerosol particles, most of the mass was in large particles of hundreds of nm in diameter, and such particle can be transported long-distances from continental anthropogenic source areas. Unlike MSA, or more accurately methane sulfonate, sulphate ($nss-SO_4^{2-}$) effectively

390   forms in the liquid phase from SO_2. Long-range transport and cloud processing may thereby explain the low correlation between MS^- and $nss-SO_4^{2-}$ in the particle phase. However, in the gas phase, we found a high correlation between MSA and SA (R^2=0.91) especially during springtime after the decay of Arctic Haze. This indicates that during the post-haze time, gas-phase SA and MSA originate primarily from DMS oxidation and the contribution of anthropogenic sulfur dioxide (SO_2) pollution to SA production is small. It is therefore natural that the temporal evolution of MSA and SA appeared to follow

395   similar patterns as probable atmospheric DMS mixing ratio which in this work is proxied by pelagic Chl-a and PP.

Chl-a and PP concentrations in the Barents Sea were higher than in the Greenland Sea during April and May, while this pattern was inverted during June–July. These features can be at least partly explained by the early phytoplankton bloom in the Barents Sea due to the earlier melting of sea ice. Despite the larger melting of the Greenland sea ice (the portion of sea ice close to Svalbard) starting later, a certain portion of Greenland sea ice already starts to melt in April, determining the shape of the Chl-

400   a and PP peaks, characterized by a slow increase in April-May and higher concentration in June. PP follows the same seasonal pattern as Chl-a, but the differences in the absolute values of PP between the two oceanic regions during the blooms are small. This could be due to a photo-adaptation process, i.e. different amounts of Chl-a in the cell as a function of photosynthetic active radiation (PAR) availability (Kirk, 1994).

405

From the April–May period to the June–July period, the correlation between the ocean color data (Chl-a and PP) and MSA decreased in the Barents Sea and increased in the Greenland Sea, which establishes a direct relationship between the sea ice melting, phytoplankton bloom and MSA. A similar pattern was observed for SA, probably because both MSA and SA originate from DMS oxidation. In spring, the HIO_3 concentration had a strong correlation with the ocean color parameters (Chl-a and PP) in the Greenland Sea, which could suggest pelagic phytoplankton as a source of iodine. However, these correlations decreased notably during the summertime. Based on Sipilä et al. (2016), we can speculate that the source of HIO_3 would rather be the sea ice and, despite the correlation between HIO_3 and ocean color parameters (Chl-a and PP), there is no causal connection between them (or between HIO_3 and open ocean phytoplankton in general). Sea ice melting (decrease of areal coverage) starts during June–July, while the sea ice extent is roughly constant during April–May (springtime) in the Greenland Sea.Among the trace gases studied here, the HOM concentration had the lowest correlation with the ocean parameters in both seasons, suggesting that HOM have completely different sources than MSA, SA and HIO_3. HOM can originate e.g. from oxidation of VOCs from terrestrial ecosystems, including soil, or VOCs or SVOCs transported from the Eurasian continent.

The significant correlations between the small-particle (10–50 nm) concentration and Chl-a and PP were found during the springtime in both Barents Sea and Greenland Sea, whereas correlations during summertime (June-July) were extremely low in both seas. Such strong correlations mean that the phytoplankton productivity has a strong impact on small-particle formation in the spring season, and that MSA and SA arising from biogenic productivity are associated with this phenomenon. These processes are mainly active in spring, whereas small-particles are not solely related to ocean color parameters in summertime, as demonstrated by low correlations during that time of the year. Explaining the summertime 10-50 nm particle concentrations (and inevitably associated NPF) likely requires other vapours, such as HOMs that cover the effect of plankton-related MSA and SA. The concentration of 100–450 nm particles anti-correlated with the ocean color data during springtime. This shows that these larger particles are not related to biogenic activity, but are likely of anthropogenic origin and are diluted upon the breakdown of polar vortex and clearing of Arctic Haze.

While the correlation analysis alone does not provide a direct connection between phytoplankton emissions and atmospheric constituents, our results provide strong support to the hypothesis that MSA, SA and small-particle concentrations in the Svalbard area are directly linked to ocean biological activity and sea ice melting during springtime. Climate change can have adverse effects on sea ice properties and marine biology, and consequently on the emissions of DMS and concentrations of particle precursor vapours and new particles. Further research is required to quantify the present-day and to predict the future contributions of marine DMS in the arctic aerosol, and especially in the CCN concentration which largely modifies cloud radiative properties and radiative balance of the Arctic atmosphere.

Atmospheric
Chemistry
and Physics
Discussions

Data availability

Mass spectrometer and SMPS data related to this article are available upon request to the corresponding author. Rest of the
440 data are available for download from:

http://www.esa-oceancolour-cci.org (Chl-a data),

http://www.science.oregonstate.edu/ocean.productivity/index.php (PP data),

https://nsidc.org/ (sea ice extent).

Supplement link

445 The link to the supplement will be included by Copernicus, if applicable.

Team list

Author contribution

MS, SB, RT designed the gas phase and particle phase experiments respectively. LJB processed and analysed the mass
spectrometric data. MM, SJ and TN preformed the calculations. MS conceptualized the idea of connecting marine biology
450 and atmospheric processes. GN helped MM to analyses the satellite data procurement. KL and VMK gave many important
advices to improve work quality. All authors contributed in the data interpretation and commented the manuscript.

Competing interests

 The authors declare that they have no conflict of interest.

Special issue statement

455 The statement on a corresponding special issue will be included by Copernicus, if applicable.

Acknowledgements

References

Allan, J. D., Williams, P. I., Najera, J., Whitehead, J. D., Flynn, M. J., Taylor, J. W., Liu, D., Darbyshire, E., Carpenter, L. J.,
465 Chance, R., Andrews, S. J., Hackenberg, S. C., McFiggans, G.: Iodine observed in new particle formation events in the Arctic
atmosphere during ACCACIA, Atmos. Chem. Phys., 15, 5599–5609, https://doi.org/10.5194/acpd-14-28949-2014, 2015.

Atkinson, H. M., Huang, R.-J., Chance, R., Roscoe, H. K., Hughes, C., Davison, B., Schönhardt, A., Mahajan, A. S., Saiz-Lopez, A., Hoffmann, T., Liss, P. S.: Iodine emissions from the sea ice of the Weddell Sea, Atmos. Chem. Phys., 12, 11229-
470   11244, https://doi.org/10.5194/acp-12-11229-2012, 2012.

Baccarini, A., Karlsson, L., Dommen, J., Duplessis, P., Vüllers, J., Brooks, I. M., Saiz-Lopez, A., Salter, M., Tjernström, M., Baltensperger, U., Zieger, P., Schmale, J.: Frequent new particle formation over the high Arctic pack ice by enhanced iodine emissions, Nat. Commun., 11, 4924, https://doi.org/10.1038/s41467-020-18551-0, 2020.

475

Bates, T.S., Charlson, R.J., Gammon, R.H.: Evidence for the climatic role of marine biogenic sulphur, Nature., 329, 319–321, https://doi.org/10.1038/329319a0, 1987.

Becagli, S.; Amore, A.; Caiazzo, L.; Iorio, T.D.; Sarra, A.d.; Lazzara, L.; Marchese, C.; Meloni, D.; Mori, G.; Muscari, G.;
480   Nuccio, C.; Pace, G.; Severi, M.; Traversi, R.: Biogenic Aerosol in the Arctic from Eight Years of MSA Data from Ny Ålesund (Svalbard Islands) and Thule (Greenland). Atmosphere., 10, 349, https://doi.org/10.3390/atmos10070349, 2019.

Becagli, S., Lazzara, L., Fani, F., Marchese, C., Traversi, R., Severi, M., di Sarrac, A., Sferlazzod, D., Piacentinoe, S., Bommaritoe, C., Dayanf, U., Udisti, R.: Relationship between methanesulfonate (MS−) in atmospheric particulate and
485   remotely sensed phytoplankton activity in oligo-mesotrophic central Mediterranean Sea, Atmos. Environ., 79, 681-688, https://doi.org/10.1016/j.atmosenv.2013.07.032, 2013.

Becagli, S., Lazzara, L., C., Marchesec Dayan, U., Ascanius, S.E., Cacciani, M., Caiazzo, L., Di Biagio, C., Di Iorio, T., Di Sarra, A., Eriksen, P., Fani, F., Giardi, F., Meloni, D., Muscari, G., Pace, G., Severi, M., Traversi, R., Udisti, R.: Relationships
490   linking primary production, sea ice melting, and biogenic aerosol in the Arctic , Atmos. Environ., 135, 1-15, https://doi.org/10.1016/j.atmosenv.2016.04.002, 2016.

Beck, L. J., Sarnela, N., Junninen, H., Hoppe, C. J. M., Garmash, O., Bianchi, F., Riva, M., Rose, C., Peräkylä, O., Wimmer, D., Kausiala, O., Jokinen, T., Ahonen, L., Mikkilä, J., Hakala, J., He, X., Kontkanen, J., Wolf, K. K. E., Cappelletti, D.,
495   Mazzola, M., Traversi, R., Petroselli, C., Viola, A. P., Vitale, V., Lange, R., Massling, A., Nøjgaard, J. K., Krejci, R., Karlsson, L., Zieger, P., Jang, S., Lee, K., Vakkari, V., Lampilahti, J., Thakur, R. C., Leino, K., Kangasluoma, J., Duplissy, E., Siivola, E., Marbouti, M., Tham, Y. J., Saiz-Lopez, A., Petäjä, T., Ehn, M., Worsnop, D. R., Skov, H., Kulmala, M., Kerminen, V., and Sipilä, M.: Differing Mechanisms of New Particle Formation at Two Arctic Sites, Geophys. Res. Lett., 48, 1–11, https://doi.org/10.1029/2020GL091334, 2021.

500

Bianchi, F., Kurtén, T., Riva, M., Mohr, C., Rissanen, M. P., Roldin, P., Berndt, T., Crounse, J. D., Wennberg, P. O., Mentel, T. F., Wildt, J., Junninen, H., Jokinen, T., Kulmala, M., Worsnop, D. R., Thronton, J. A., Donahue, N., Kjaergaard, H. G., and Ehn, M.: Highly oxygenated organic molecules (HOM) from gas-phase autoxidation involving peroxy radicals: A key contributor to atmospheric aerosol, Chem. Rev., 119, 3472–3509, https://doi.org/10.1021/acs.chemrev.8b00395, 2019.

505   Boucher, O., Randall, D., Artaxo, P., Bretherton, C., Feingold, G., Forster, P., Kerminen, V.-M., Kondo, Y., Liao, H., Lohmann, U., Rasch, P., Satheesh, S., Sherwood, S., Stevens, B., and Zhan, X.: Clouds and Aerosols, in: Climate Change 2013: The Physical Science Basis. Contribution of Working Group I to the Fifth Assessment Report of the Intergovernmental Panel on Climate Change, edited by: Stocker, T., Qin, D., Plattner, G., Tignor, M., Allen, S., Boschung, J., Nauels, A., Xia, Y., Bex, V., and Midgley, P., Cambridge University Press, Cambridge, United Kingdom and New York, NY, USA, 2013.

510

Charlson, R. J., Lovelock, J. E., Andreae, M. O. and Warren, S. G.: Oceanic phytoplankton, atmospheric sulphur, cloud albedo and climate. Nature., 326, 655–661, https://doi.org/10.1038/326655a0, 1987.

Croft, B., Martin, R. V., Leaitch, W. R., Tunved, P., Breider, T. J., D'Andrea, S. D., and Pierce, J. R.: Processes controlling
515   the annual cycle of Arctic aerosol number and size distributions, Atmos. Chem. Phys., 16, 3665–3682, https://doi.org/10.5194/acp-16-3665-2016, 2016.

Dall'Osto, M., Beddows, D. C. S., Tunved, P., Harrison, R. M., Lupi, A., Vitale, V., Becagli, S., Traversi, R., Park, K.-T., Yoon, Y. J., Massling, A., Skov, H., Lange, R., Strom, J., and Krejci, R.: Simultaneous measurements of aerosol size
520   distributions at three sites in the European high Arctic, Atmos. Chem. Phys., 19, 7377–7395, https://doi.org/10.5194/acp-19-7377-2019, 2019.

Dall'Osto, M., Beddows, D. C. S., Tunved, P., Krejci, R., Ström, J., Hansson, H.-C., Yoon, Y. J., Park, K.-T., Becagli, S., Udisti, R., Onasch, T., O'Dowd, C. D., Simó, R., and Harrison, R. M.: Arctic sea ice melt leads to atmospheric new particle
525   formation, Sci. Rep., 7, 3318, https://doi.org/10.1038/s41598-017-03328-1, 2017.

Dall'Osto, M., Geels, C., Beddows, D. C. S., Boertmann, D., Lange, R., Nøjgaard, J. K., Harrison, R. M., Simo, R., Skov, H., and Massling, A.: Regions of open water and melting sea ice drive new particle formation in North East Greenland, Sci. Rep., 8, 1– 10, https://doi.org/10.1038/s41598-018-24426-8, 2018.

530

Draxler, R.R., and Hess, G.D.: An Overview of the HYSPLIT_4 Modelling System for Trajectories, Dispersion on and Deposition. Aust. Meteorol. Mag., 47, 295-308, 1998.

Ehn, M., Kleist, E., Junninen, H., Petäjä, T., Lönn, G., Schobesberger, S., Dal Maso, M., Trimborn, A., Kulmala, M., Worsnop, D. R., Wahner, A., Wildt, J., & Mentel, T. F.: Gas phase formation of extremely oxidized pinene reaction products in chamber and ambient air. Atmos. Chem. Phys., 12, 5113-5127, https://doi.org/10.5194/acp-12-5113-2012, 2012.

Ehn, M., Thornton, J. A., Kleist, E., Sipila, M., Junninen, H., Pullinen, I., Springer, M., Rubach, F., Tillmann, R., Lee, B., Lopez-Hilfiker, F., Andres, S., Acir, I. H., Rissanen, M., Jokinen, T., Schobesberger, S., Kangasluoma, J., Kontkanen, J., Nieminen, T., Kurten, T., Nielsen, L. B., Jorgensen, S., Kjaer-gaard, H. G., Canagaratna, M., Maso, M. D., Berndt, T., Petaja,T., Wahner, A., Kerminen, V. M., Kulmala, M., Worsnop, D. R., Wildt, J., and Mentel, T. F.: A large source of low-volatility secondary organic aerosol, Nature, 506, 476–479, https://doi.org/10.1038/nature13032, 2014.

Gordon, H., Kirkby, J., Baltensperger, U., Bianchi, F., Breitenlechner, M., Curtius, J., Dias, A., Dommen, J., Donahue, N. M., Dunne, E. M., Duplissy, J., Ehrhart, S., Flagan, R. C., Frege, C., Fuchs, C., Hansel, A., Hoyle, C. R., Kulmala, M., Kürten, A., Lehtipalo, K., Makhmutov, V., Molteni, U., Rissanen, M. P., Stozkhov, Y., Tröstl, J., Tsagkogeorgas, G., Wagner, R., Williamson, C., Wimmer, D., Winkler, P. M., Yan, C., and Carslaw, K. S.: Causes and importance of new particle formation in the present-day and preindustrial atmospheres, J. Geophys. Res.-Atmos., 122, 8739–8760, https://doi.org/10.1002/2017JD026844, 2017.

Green, T. K., and Hatton, A. D.: The Claw Hypothesis: A NewPerspective on the Role of Biogenic Sulphur in the Regula-tion of Global Climate, Oceanogr. Mar. Biol., 52, 315–336, https://doi.org/10.1201/b17143-7, 2014.

He, X.-C., Tham, Y. J., Dada, L., Wang, M., Finkenzeller, H., Stolzenburg, D., Iyer, S., Simon, M., Shen, J., Rörup, B., Ris-sanen, M., Schobesberger, S., Baalbaki, R., Wang, D. S., Koenig, T. K., Jokinen, T., Sarnela, N., Beck, L., Almeida, J., Kürten, A., Amanatidis, S., Amorim, A., Ataei, F., Baccarini, A., Bertozzi, B., Bianchi, F., Brilke, S., Caudillo, L., Chen, D., Chiu, R., Chu, B., Dias, A., Ding, A., Dommen, J., Duplissy, J., El Haddad, I., Carracedo, L. G., Granzin, M., Hansel, A., Heinritzi, M., Hofbauer, V., Junninen, H., Kangasluoma, J., Kemppainen, D., Kim, C., Kong, W., Krechmer, J. E., Kvashnin, A., Laiti-nen, T., Lamkaddam, H., Lee, C. P., Lehtipalo, K., Leiminger, M., Li, Z., Makhmutov, V., Manninen, H. E., Marie, G., Marten, R., Mauldin, R. L., Mentler, B., Möhler, O., Müller, T., Nie, W., Onnela, A., Petäjä, T., Pfeifer, J., Philippov, M., Ranjithku-mar, A., Saiz-López, A., Salma, I., Scholz, W., Schuchmann, S., Schulze, B., Steiner, G., Stozhkov, Y., Tauber, C., Tomé, A., Thakur, R. C., Väisänen, O., Vazquez-Pufleau, M., Wagner, A. C., Wang, Y., Weber, S. K., Winkler, P. M., Wu, Y., Xiao, M., Yan, C., Ye, Q., Ylisirniö, A., Zauner-Wieczorek, M., Zha, Q., Zhou, P., Flagan, R. C., Curtius, J., Baltensperger, U., Kulmala, M., Kerminen, V.-M., Kurtén, T., Donahue, N. M., Volkamer, R., Kirkby, J., Worsnop, D. R., and Sipilä, M.: Role of iodine oxoacids in atmospheric aerosol nucleation, Science, 371, 589– 595, https://doi.org/10.1126/science.abe0298, 2021.

Hynes, A. J., Wine, P. H., and Semmes, D. H.: Kinetics and mechanism of hydroxyl reactions with organic sulphides. J. Phys. Chem., 90, 4148−4156, https://doi.org/10.1021/j100408a062 , 1986.

570   Jang, S., Park, K.-T., Lee, K., and Suh, Y.-S.: An analyticalsystem enabling consistent and long-term measurement of atmospheric dimethyl sulphide, Atmos. Environ., 134, 217–223, https://doi.org/10.1016/j.atmosenv.2016.03.041, 2016.

Jokinen, T., Sipilä, M., Junninen, H., Ehn, M., Lönn, G., Hakala, J., Petäjä, T., Mauldin III, R. L., Kulmala, M., and Worsnop, D. R.: Atmospheric sulphuric acid and neutral cluster measurements using CI-APi-TOF, Atmos. Chem. Phys., 12, 4117–4125,
575   https://doi.org/10.5194/acp-12-4117-2012, 2012.

Jokinen, T., Sipilä, M., Kontkanen, J., Vakkari, V., Tisler, P., Duplissy, E.-M., Junninen, H., Kangasluoma, J., Manninen, H. E., Petäjä, T., Kulmala, M., Worsnop, D. R., Kirkby, J., Virkkula, A., Kerminen, V.-M.: Ion-induced sulfuric acid–ammonia nucleation drives particle formation in coastal Antarctica, Science Advances., 4, 9744, https://doi.org/10.1126/sciadv.aat9744,
580   2018.

Junninen, H., Ehn, M., Petäjä, T., Luosujärvi, L., Kotiaho, T., Kostiainen, R., Rohner, U., Gonin, M., Fuhrer, K., Kulmala, M., and Worsnop, D. R.: A high-resolution mass spectrometer to measure atmospheric ion composition, Atmos. Meas. Tech., 3, 1039–1053, https://doi.org/10.5194/amt-3-1039-2010, 2010.

585

Kirk, J.T.O.: Light and Photosynthesis in Aquatic Ecosystems. 3rd ed. Cambridge University Press, 1994.

Kirkby, J., Curtius, J., Almeida, J., Dunne, E., Duplissy, J., Ehrhart, S., Franchin, A., Gagné, S., Ickes, L., Kürten, A., Kupc, A., Metzger, A., Riccobono, F., Rondo, L., Schobesberger, S., Tsagko-georgas, G., Wimmer, D., Amorim, A., Bianchi, F.,
590   Breitenlech-ner, M., David, A., Dommen, J., Downard, A., Ehn, M., Flagan, R. C., Haider, S., Hansel, A., Hauser, D., Jud, W., Junni-nen, H., Kreissl, F., Kvashin, A., Laaksonen, A., Lehtipalo, K., Lima, J., Lovejoy, E. R., Makhmutov, V., Mathot, S., Mikkilä, J., Minginette, P., Mogo, S., Nieminen, T., Onnela, A., Pereira, P., Petäjä, T., Schnitzhofer, R., Seinfeld, J. H., Sipilä, M., Stozhkov, Y., Stratmann, F., Tomé, A., Vanhanen, J., Viisanen, Y., Vrtala, A., Wagner, P. E., Walther, H., Weingartner, E., Wex, H., Winkler, P. M., Carslaw, K. S., Worsnop, D. R., Baltensperger, U., and Kulmala, M.: Role of
595   sulphuric acid, ammonia and galactic cosmic rays in atmospheric aerosol nucleation, Nature, 476, 429–435, https://doi.org/10.1038/nature10343, 2011.

Kirkby, J., Duplissy, J., Sengupta, K., Frege, C., Gordon, H., Williamson, C., Heinritzi, M., Simon, M., Yan, C., Almeida, J., Tröstl, J., Nieminen, T., Ortega, I. K., Wagner, R., Adamov, A., Amorim, A., Bernhammer, A.-K., Bianchi, F., Breitenlechner,
600   M., Brilke, S., Chen, X., Craven, J., Dias, A., Ehrhart, S., Flagan, R. C., Franchin, A., Fuchs, C., Guida, R., Hakala, J., Hoyle,

C. R., Jokinen, T., Junninen, H., Kangasluoma, J., Kim, J., Krapf, M., Kürten, A., Laaksonen, A., Lehtipalo, K., Makhmutov, V., Mathot, S., Molteni, U., Onnela, A., Peräkylä, O., Piel, F., Petäjä, T., Praplan, A. P., Pringle, K., Rap, A., Richards, N. A. D., Riip-inen, I., Rissanen, M. P., Rondo, L., Sarnela, N., Schobesberger, S., Scott, C. E., Seinfeld, J. H., Sipilä, M., Steiner, G., Stozhkov, Y., Stratmann, F., Tomé, A., Virtanen, A., Vogel, A. L., Wagner, A. C., Wagner, P. E., Weingartner, E.,
605 Wimmer, D., Winkler, P. M., Ye, P., Zhang, X., Hansel, A., Dommen, J., Donahue, N. M., Worsnop, D. R., Baltensperger, U., Kulmala, M., Carslaw, K. S., and Curtius, J.: Ion-induced nucleation of pure biogenic particles, Nature, 533, 521–526, https://doi.org/10.1038/nature17953, 2016.

Li, S. M., and Barrie, L. A.: Biogenic sulfur aerosol in the Arctic troposphere: 1. Contributions to total sulfate.
610 J. Geophys. Res-Atmos, 98, 20613-20622, https://doi.org/10.1029/93JD02234, 1993b.

Li, S. M., Barrie, L. A., Talbot, R. W., Harriss, R. C., Davidson, C. I., & Jaffrezo, J. L.: Seasonal and geographic variations of methanesulfonic acid in the Arctic troposphere, Atmos. Environ. Part A. General Topics., 27, 3011-3024, https://doi.org/10.1016/0960-1686(93)90333-T, 1993a.
615

Mahajan, A.S., Shaw, M., Oetjen, H., Hornsby, K. E., Carpenter, L. J., Kaleschke, L., Tian, X., Lee, J. D., Moller, S. J., Edwards, P., Commane, R., Ingham, T., Heard, D. E., Plane, M.C.: Evidence of reactive iodine chemistry in the Arctic boundary layer. J. Geophys. Res-Atmos.,115, D20303, https://doi.org/10.1029/2009JD013665, 2010.

620 Mäkelä, J. M., Hoffmann, T., Holzke, C., Väkevä, M., Suni, T., Mattila, T., Aalto, P. P., Tapper, U., Kauppinen, E. I., and O'Dowd, C. D., Biogenic iodine emissions and identification of end-products in coastal ultrafine particles during nucleation bursts, J. Geophys. Res-Atmos., 107, 8110, https://doi.org/10.1029/2001JD000580, 2002.

Matrai, P. A., Vernet, M., Wassmann, P.: Relating temporal and spatial patterns of DMSP in the Barents Sea to phytoplankton
625 biomass and productivity. J. Mar. Syst., 67, 83-101, https://doi.org/10.1016/j.jmarsys.2006.10.001, 2007.

Moore, R. M., Webb, M., Tokarczyk, R., Wever, R.: Bromoperoxidase and iodoperoxidase enzymes and production of halogenated methanes in marine diatom cultures, J. Geophys. Res-Oceans., 101, 20899-20908, https://doi.org/10.1029/96JC01248, 1996.
630

O'Dowd, Colin D., Jose L. Jimenez, Roya Bahreini, Richard C. Flagan, John H. Seinfeld, Kaarle Hämeri, Liisa Pirjola, Markku Kulmala, S. Gerard Jennings & Thorsten Hoffmann. 2002. Nature 417: 632–636. Doi: https://doi.org/10.1038/nature00775

Atmospheric
Chemistry
and Physics
Discussions

635 Park, K.-T., Jang, S., Lee, K., Yoon, Y. J., Kim, M.-S., Park, K., Cho, H.-J., Kang, J.-H., Udisti, R., Lee, B.-Y., and Shin, K.-H.: Observational evidence for the formation of DMS-derived aerosols during Arctic phytoplankton blooms, Atmos. Chem. Phys., 17, 9665–9675, https://doi.org/10.5194/acp-17-9665-2017, 2017.

Park, K.-T., Lee, K., Kim, T. W., Yoon, Y. J., Jang, E. H., Jang, S., Lee, B.-Y., and Hermansen, O.: Atmospheric DMS in the Arctic Ocean and its relation to phytoplankton biomass, Global. Biogeochem. Cy., 32, 351–359,
640 https://doi.org/10.1002/2017GB005805, 2018.

Park, K.-T., Lee, K., Yoon, Y.-J., Lee, H.-W., Kim, H.-C., Lee, B.-Y., Hermansen, O., Kim, T.-W., Holmén, K.: Linking atmospheric dimethyl sulfide (DMS) and the Arctic Ocean spring bloom, Geophys. Res. Lett., 40, 155–160, https://doi.org/10.1029/2012GL054560, 2013.

645
Perrette, M., Yool, A., Quartly, G. D., and Popova, E. E.: Near-ubiquity of ice-edge blooms in the Arctic, Biogeosciences, 8, 515–524, https://doi.org/10.5194/bg-8-515-2011, 2011.

Plummer, S., Lecomte, P., and Doherty, M.: The ESA Climate Change Initiative (CCI): A European contribution to the
650 generation of the Global Climate Observing System. Remote. Sens. Environ., 203, 2–8, https://doi.org/10.1016/j.rse.2017.07.014, 2017.

Quinn, P. K., & Bates, T. S.: The case against climate regulation via oceanic phytoplankton sulfur emissions. Nature, 480, 51–56, https://doi.org/10.1038/nature10580, 2011.

655
Quinn, P.K., Shaw, G., Andrews, E., Dutton, E.G., Ruoho-Airola, T., Gong, S.L.: Arctic haze: current trends and knowledge gaps. Tellus. Ser B., 59, 99-114, https://doi.org/10.1111/j.1600-0889.2006.00238.x, 2007.

Rat'kova, T. N., Wassmann, P.: Seasonal variation and spatial distribution of phyto- and protozooplankton in the central
660 Barents Sea. J. Marine. Syst., 38, 47-75, https://doi.org/10.1016/S0924-7963(02)00169-0, 2002.

Read, K. A., Lewis, A. C., Bauguitte, S., Rankin, A. M., Salmon, R. A., Wolff, E. W., Saiz-Lopez, A., Bloss, W. J., Heard, D. E., Lee, J. D., and Plane, J. M. C.: DMS and MSA measurements in the Antarctic Boundary Layer: impact of BrO on MSA
665 production, Atmos. Chem. Phys., 8, 2985–2997, https://doi.org/10.5194/acp-8-2985-2008, 2008.

Saiz-Lopez, A., Blaszczak-Boxe, C. S., and Carpenter, L. J.: A mechanism for biologically induced iodine emissions from sea ice. Atmos. Chem. Phys., 15, 9731–9746, https://doi.org/10.5194/acp-15-9731-2015, 2015.

670 Sharma, S., Chan, E., Ishizawa, M., Toom-Sauntry, D., Gong, S.L., Li, S.M.D., Tarasick, W., Leaitch, W.R., Norman, A., Quinn, P.K., Bates, T.S., Levasseur, M., Barrie, L.A., Maenhaut, W.: Influence of transport and ocean ice extent on biogenic aerosol sulfur in the Arctic atmosphere. J. Geophys. Res-Atmos., 117, D12, http://dx.doi.org/10.1029/2011JD017074, 2012.

Simo, R.: Production of atmospheric sulfur by oceanic plankton: biogeo-chemical, ecological and evolutionary links. Trends.
675 Ecol. Evol., 16, 287-294, https://doi.org/10.1016/S0169-5347(01)02152-8, 2001.

Sipilä, M., Sarnela, N., Jokinen, T., Henschel, H., Junninen, H., Kontkanen, J., Richters, S., Kangasluoma, J., Franchin, A., Peräkylä, O., Rissanen, M. P., Ehn, M., Vehkamäki, H., Kurten, T., Berndt, T., Petäjä, T., Worsnop, D., Ceburnis, D., Kerminen, V. M., Kulmala, M. and O'Dowd, C.: Molecular-scale evidence of aerosol particle formation via sequential addition
680 of HIO3, Nature, 537(7621), 532–534, https://doi.org/10.1038/nature19314, 2016.

Stefels, J., Steinke, M., Turner, S., Malin, G., & Belviso, S.: Environmental constraints on the production and removal of the climatically active gas dimethyl sulphoxide (DMS) and implications for ecosystem modelling, Biogeochemistry, 83, 245–275.
https://doi.org/10.1007/s10533-007-9091-5, 2007.
685

Stein, A. F., Draxler, R. R., Rolph, G. D., Stunder, B. J. B., Cohen, M. D. and Ngan, F.: Noaa's hysplit atmospheric transport and dispersion modeling system, Bull. Am. Meteorol. Soc., 96, 2059–2077, https://doi.org/10.1175/BAMS-D-14-00110.1, 2015.

690 Tröstl, J., Chuang, W. K., Gordon, H., Heinritzi, M., Yan, C., Molteni, U., Ahlm, L., Frege, C., Bianchi, F., Wagner, R., Simon, M., Lehtipalo, K., Williamson, C., Craven, J. S., Duplissy, J., Adamov, A., Almeida, J., Bernhammer, A.-K., Bre-itenlechner, M., Brilke, S., Dias, A., Ehrhart, S., Flagan, R. C., Franchin, A., Fuchs, C., Guida, R., Gysel, M., Hansel, A., Hoyle, C. R., Jokinen, T., Junninen, H., Kangasluoma, J., Kesk-inen, H., Kim, J., Krapf, M., Kürten, A., Laaksonen, A., Lawler, M., Leiminger, M., Mathot, S., Möhler, O., Nieminen, T., Onnela, A., Petäjä, T., Piel, F. M., Miettinen, P., Rissanen, M. P., Rondo,
695 L., Sarnela, N., Schobesberger, S., Sengupta, K., Sipilä, M., Smith, J. N., Steiner, G., Tomè, A., Virtanen, A., Wagner, A. C., Weingartner, E., Wimmer, D., Winkler, P. M., Ye, P., Carslaw, K. S., Curtius, J., Dommen, J., Kirkby, J., Kulmala, M., Riipinen, I., Worsnop, D. R., Donahue, N. M., and Bal-tensperger, U.: The role of low-volatility organic compounds in initial particle growth in the atmosphere, Nature, 533, 527–531, https://doi.org/10.1038/nature18271, 2016.

700 Wassmann, P., Reigstad, M., Haug, T., Rudels, B., Carroll, M.L., Hop, H., Gabrielsen, W.G., Falk-Petersen,

S., Denisenko, S.G., Arashkevich, E., Slagstad, D., Pavlova, O.: Food webs and carbon flux in the Barents Sea. Prog. Oceanogr., 71, 232-287, https://doi.org/10.1016/j.pocean.2006.10.003, 2006a.

Wassmann, P., Slagstad, D., Wexels Riser, C., Reigstad, M.: Modelling the ecosystem dynamics of the marginal ice zone and

705 central Barents Sea. II. Carbon flux and interannual variability. J. Marine. Syst., 59, 1-24, https://doi.org/10.1016/j.jmarsys.2005.05.006, 2006b.

Xue, J., Li, Y., Wang, X., Durbin, T. D., Johnson, K. C., Karavalakis, G., Asa-Awuku, A., Villela, M., Quiros, D., Hu, S., and Huai, T.: Comparison of vehicle exhaust particle size distributions measured by SMPS and EEPS during steady-state

710 conditions, Aerosol Sci. Technol., 49, 984–996, https://doi.org/10.1080/02786826.2015.1088146, 2015.

715

720

725

730

735

Appendix:

(a)

(b)

(c)

(d)
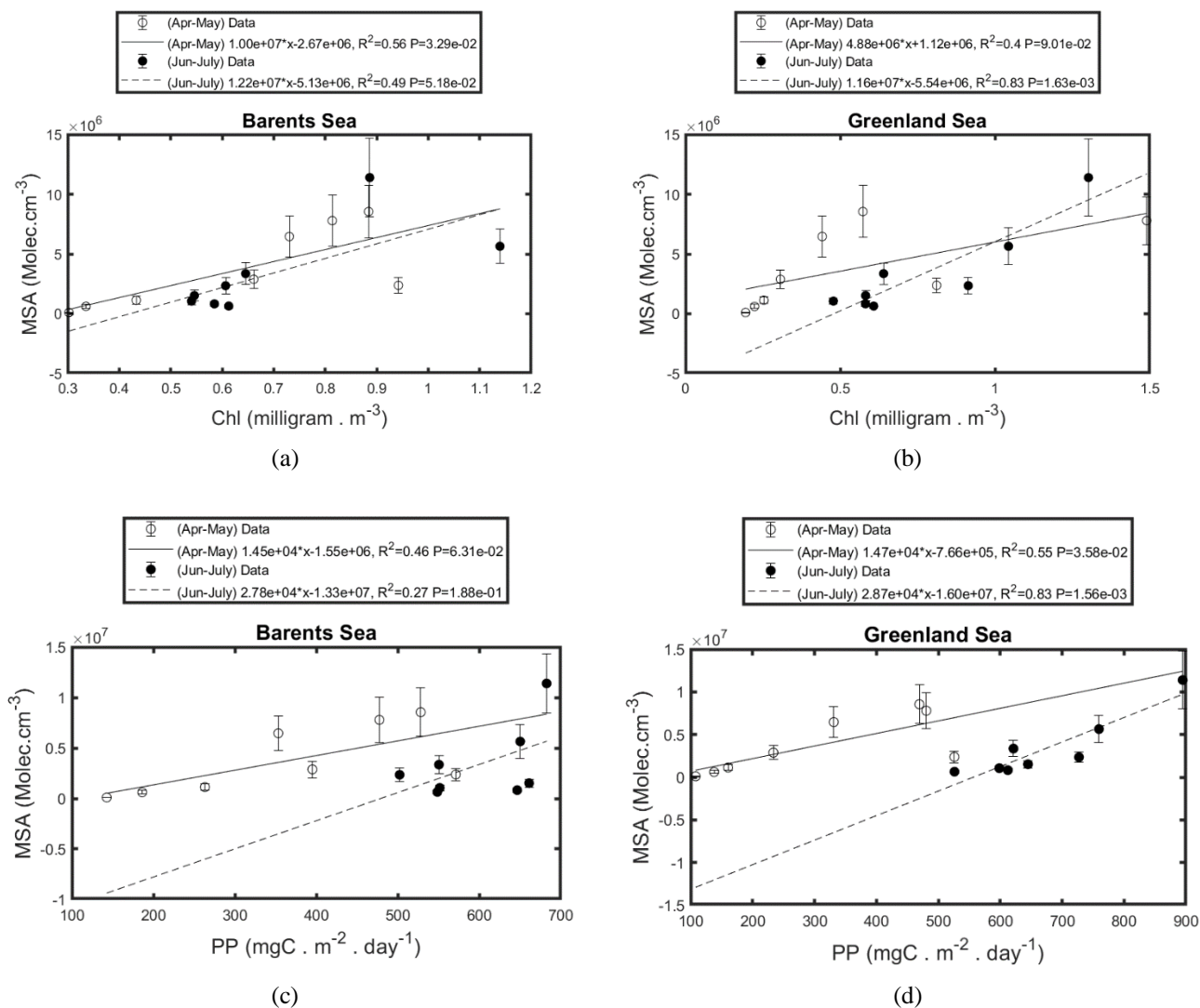
Figure A1. Scatterplot of MSA at Ny-Ålesund and Chl-a and PP for Barents Sea and Greenland Sea in the period April-may (open dots)
740   and June-July (dark circles).

745
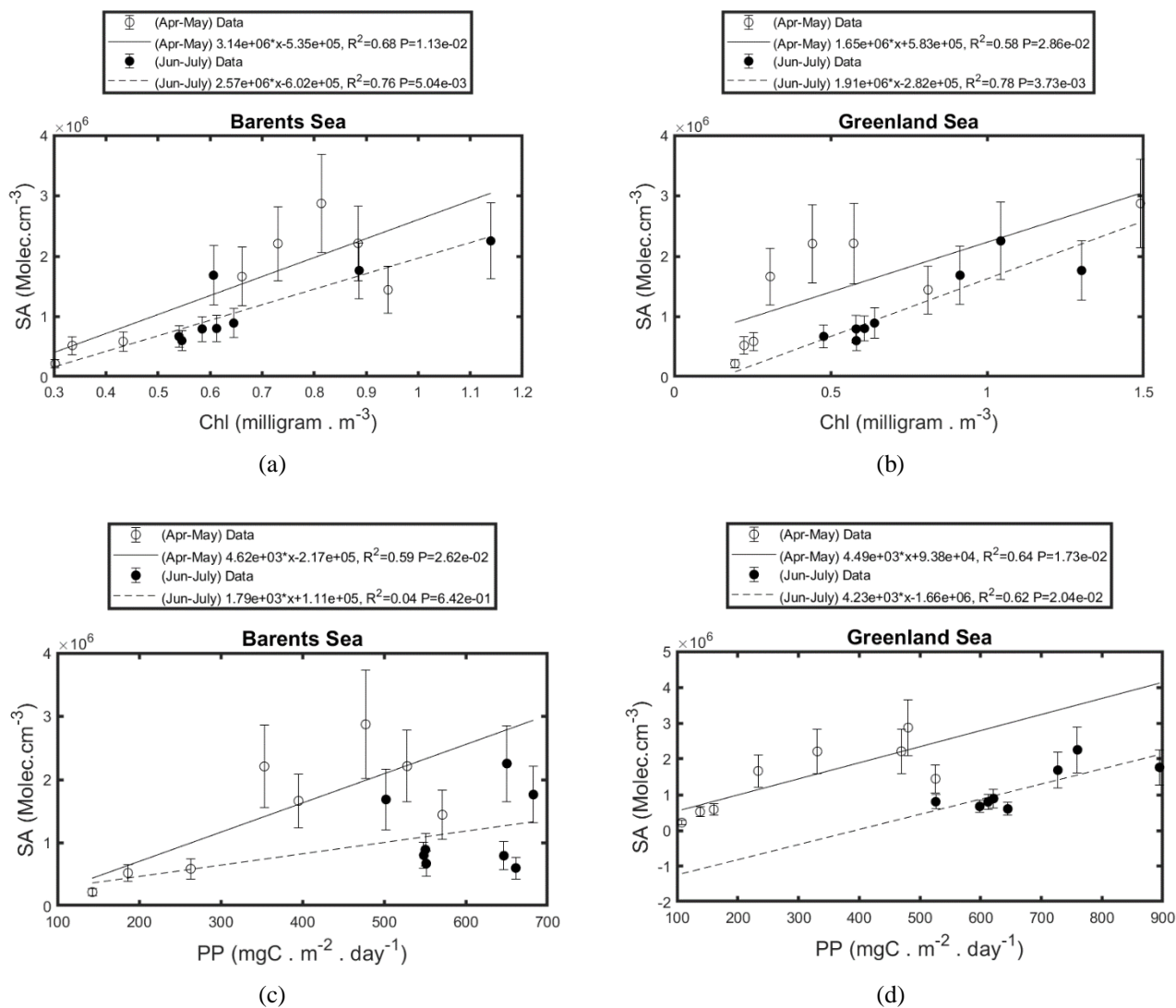
Figure A2. Scatterplot of SA at Ny Ålesund and Chl-a and PP for Barents Sea and Greenland Sea in the period April-may (open dots) and June-July (dark circles).

750

755
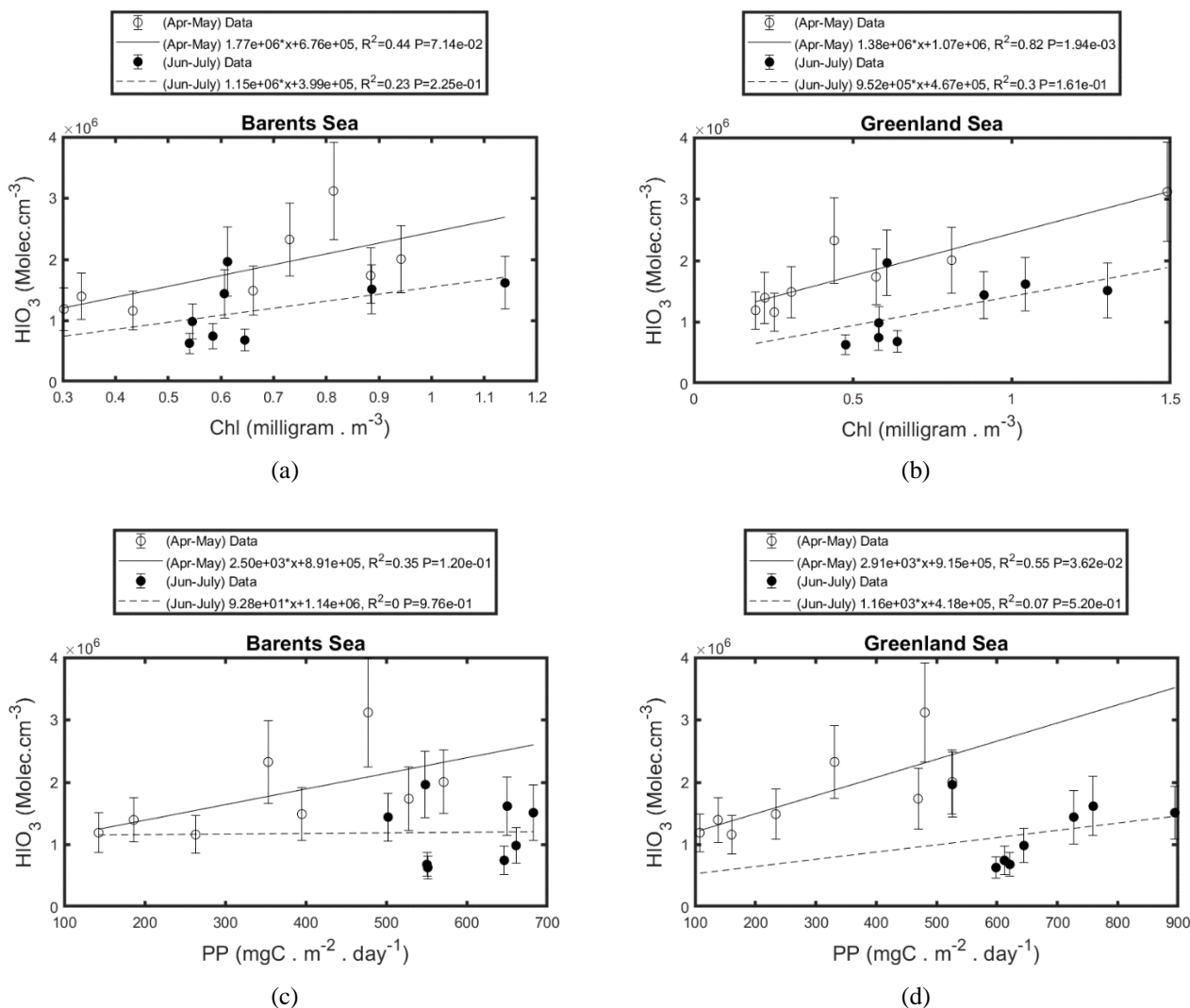
Figure A3. Scatterplot of HIO$_3$ at Ny Ålesund and Chl-a and PP for Barents Sea and Greenland Sea in the period April-may (open dots) and June-July (dark circles).

760

(a)

(b)

(c)

(d)
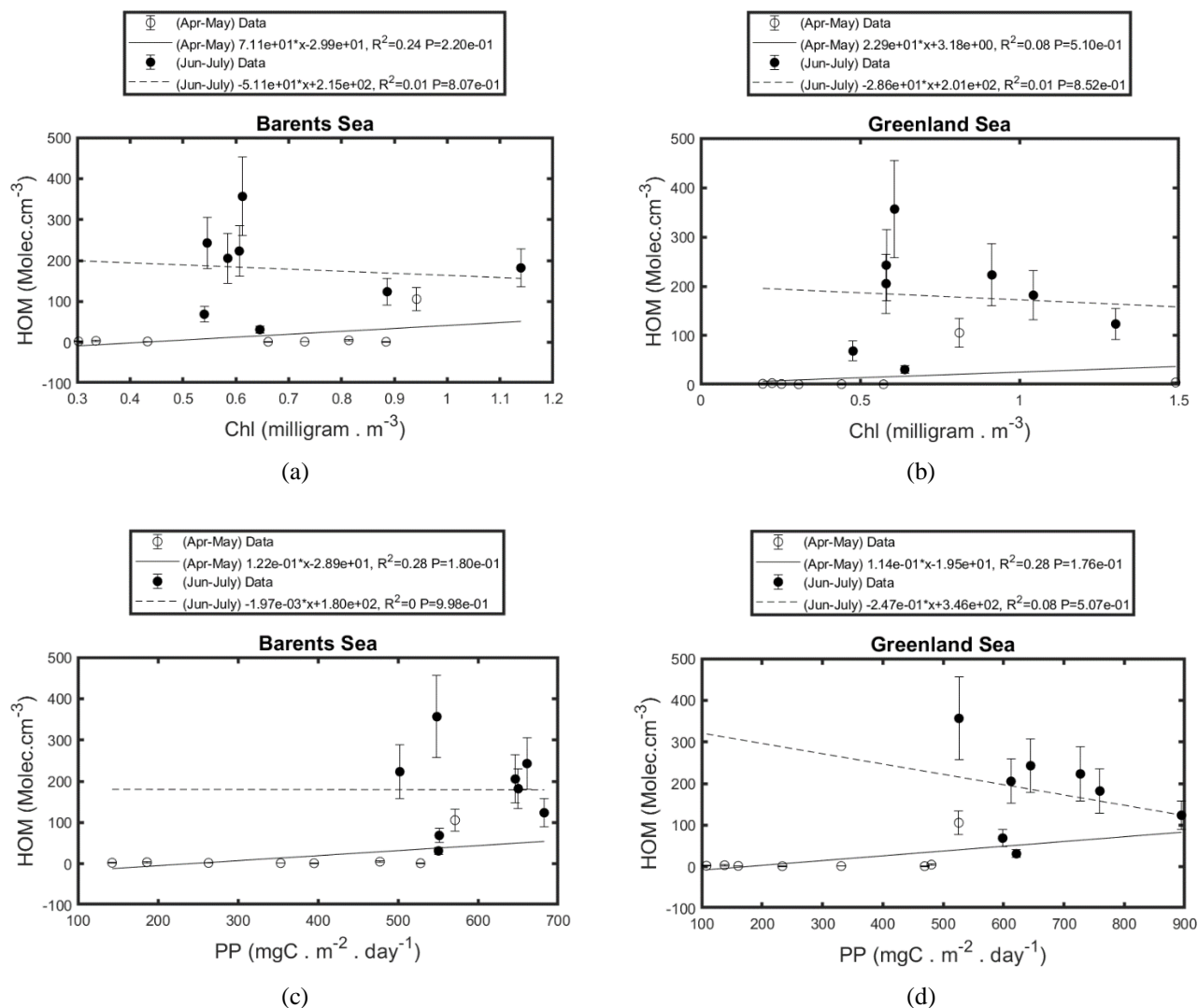
Figure A4. Scatterplot of HOM at Ny Ålesund and Chl-a and PP for Barents Sea and Greenland Sea in the period April-may (open dots) and June-July (dark circles).
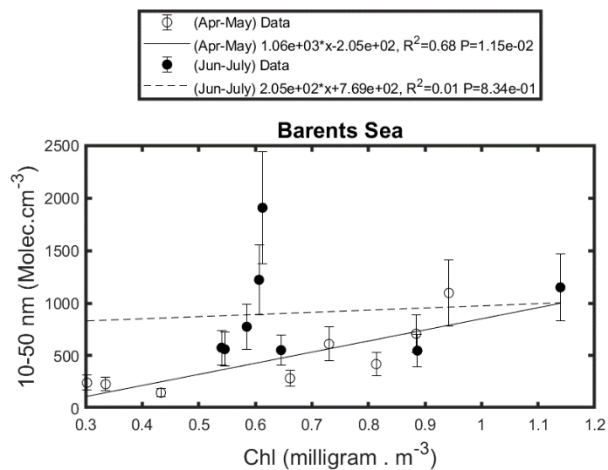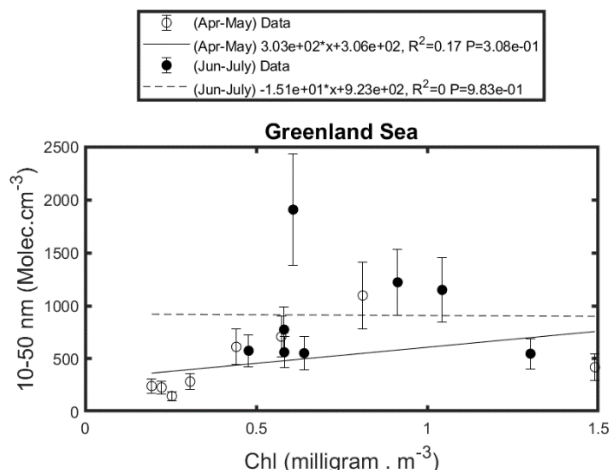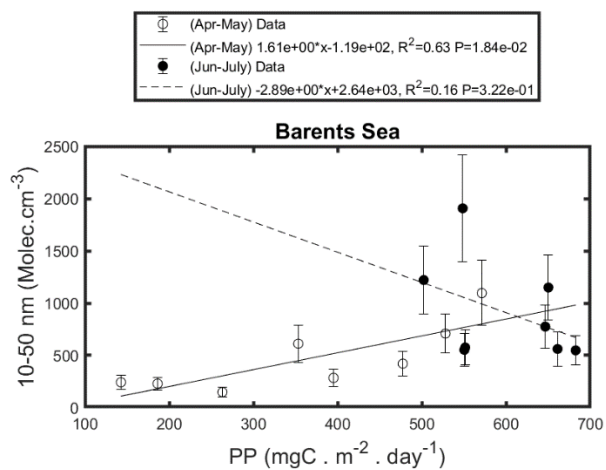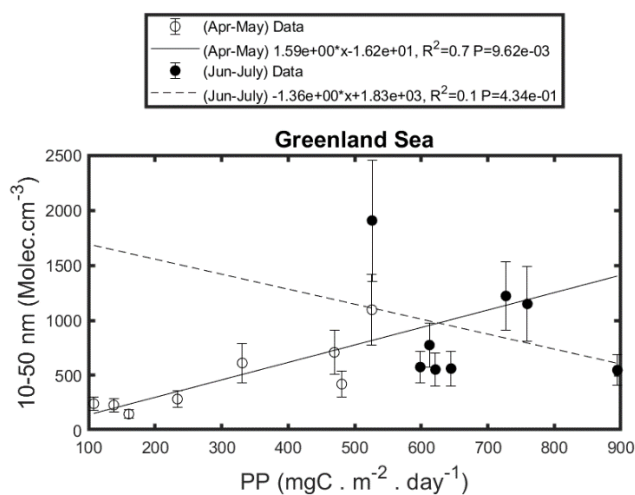
Figure A5. Scatterplot of aerosol concentration (10 - 50 nm) at Ny Ålesund and Chl-a and PP for Barents Sea and Greenland Sea in the period April-may (open dots) and June-July (dark circles).

775
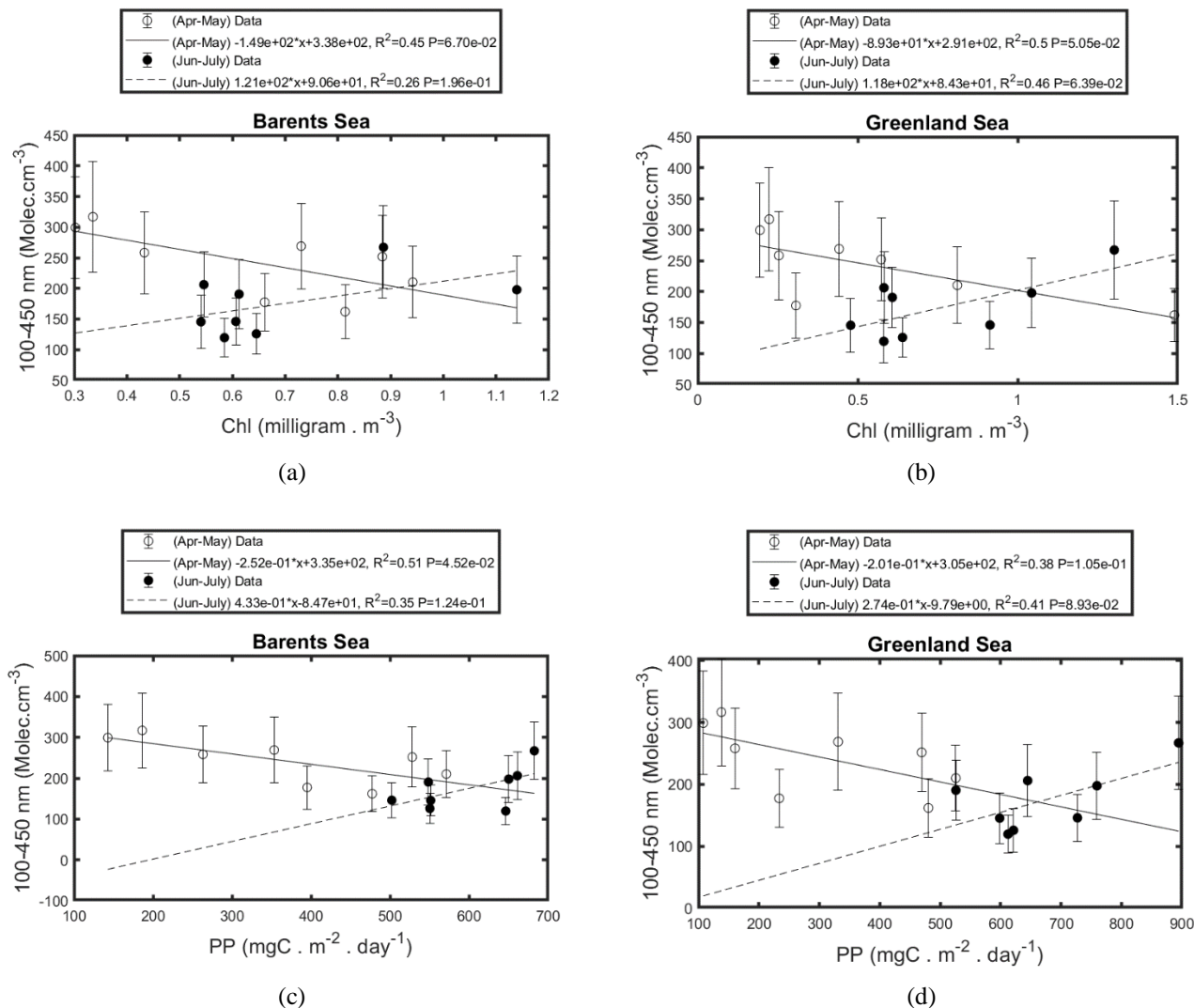
Figure A6. Scatterplot of aerosol concentration (100-450 nm) at Ny Ålesund and Chl-a and PP for Barents Sea and Greenland Sea in the period April-may (open dots) and June-July (dark circles).